HYDRATE FORMATION CONDITIONS OF METHANE HYDROGEN SULFIDE MIXTURES

A THESIS SUBMITTED TO
THE GRADUATE SCHOOL OF NATURAL AND APPLIED SCIENCES
OF
MIDDLE EAST TECHNICAL UNIVERSITY

BY

SEVTAÇ BÜLBÜL

IN PARTIAL FULFILLMENT OF THE REQUIREMENTS
FOR
THE DEGREE OF MASTER OF SCIENCE
IN
PETROLEUM AND NATURAL GAS ENGINEERING

FEBRUARY 2007

Approval of the Graduate School of Natural and Applied Sciences

Prof. Dr. Canan ÖZGEN
Director

I certify that this thesis satisfies all the requirements as a thesis for the degree of Master of Science.

Prof. Dr. Mahmut PARLAKTUNA
Head of Department

This is to certify that we have read this thesis and that in our opinion it is fully adequate, in scope and quality, as a thesis for the degree of Master of Science.

Prof. Dr. Mahmut PARLAKTUNA Co- Supervisor	Prof. Dr. Tanju MEHMETOĞLU Supervisor

Examining Committee Members

Prof. Dr. Fevzi GÜMRAH	(METU, PETE)	_____
Prof. Dr. Tanju MEHMETOĞLU	(METU, PETE)	_____
Prof. Dr. Mahmut PARLAKTUNA	(METU, PETE)	_____
Assist. Prof. Dr. Evren ÖZBAYOĞLU	(METU, PETE)	_____
Uğur KARABAKAL, MSc.	(TPAO)	_____

I hereby declare that all information in this document has been obtained and presented in accordance with academic rules and ethical conduct. I also declare that, as required by these rules and conduct, I have fully cited and referenced all material and results that are not original to this work.

Name, Last name: Sevtaç BÜLBÜL

Signature:

ABSTRACT

HYDRATE FORMATION CONDITIONS OF
METHANE HYDROGEN SULFIDE MIXTURES

Bülbül, Sevtaç
M.Sc., Department of Petroleum and Natural Gas Engineering
Supervisor: Prof. Dr. Tanju Mehmetoğlu
Co- Supervisor: Prof. Dr. Mahmut Parlaktuna

February 2007, 87 pages

The objective of this study is to determine hydrate formation conditions of methane-hydrogen sulfide mixtures. During the study, an experimental work is carried out by using a system that contains a high-pressure hydrate formation cell and pressure-temperature data is recorded in each experiment. Different H_2S concentrations and both brine and distilled water are used in the experiments and the Black Sea conditions, which are suitable for methane-hydrogen sulfide hydrate formation are examined.

Considering the pressure-temperature data obtained, hydrate equilibrium conditions are determined as well as the number of moles of free gas in the hydrate formation cell. The change in the number of moles of free gas in the hydrate formation cell with respect to time is considered as a way of determining rate of hydrate formation. Effects of H_2S concentration and salinity on hydrate formation conditions of methane-hydrogen sulfide mixtures are also studied. It is observed

that an increase in the salinity shifts the methane-hydrogen sulfide hydrate equilibrium condition to lower equilibrium temperatures at a given pressure. On the other hand, with an increase in H_2S concentration the methane hydrogen sulfide hydrate formation conditions reach higher equilibrium temperature values at a given pressure. After the study, it can be also concluded that the Black Sea has suitable conditions for hydrate formation of methane hydrogen sulfide mixtures, considering the results of the experiments.

Keyword: Hydrate, Methane-Hydrogen Sulfide Mixtures, Hydrate Formation Conditions, Black Sea

ÖZ

METAN HİDROJEN SÜLFÜR KARIŞIMLARININ
HİDRAT OLUŞUM KOŞULLARI

Bülbül, Sevtaç
Yüksek Lisans, Petrol ve Doğal Gaz Mühendisliği Bölümü
Tez Yöneticisi: Prof. Dr. Tanju Mehmetoğlu
Ortak Tez Yöneticisi: Prof. Dr. Mahmut Parlaktuna

Şubat 2007, 87 sayfa

Bu çalışmanın amacı, metan-hidrojen sülfür karışımlarının hidrat oluşum koşullarını belirlemektir. Yapılan çalışma sırasında, içinde yüksek basınçlı bir hidrat oluşum hücresi bulunan bir sistem kullanılarak deneysel çalışmalar sürdürülmüş ve basınç-sıcaklık değerleri kaydedilmiştir. Deneylerde farklı H_2S konsantrasyonları ve aynı zamanda, tuzlu su ve saf su kullanılmış ve Karadeniz'in metan-hidrojen sülfür hidratı oluşumuna uygun koşulları incelenmiştir.

Elde edilen basınç-sıcaklık verileri değerlendirilerek, hidrat oluşum hücresi içinde yer alan serbest gazın mol sayısı ile birlikte hidrat denge koşulları da belirlenmiştir. Hidrat oluşum hücresi içinde yer alan serbest gazın mol sayısının zamana bağlı olarak değişiminin incelenmesi, hidrat oluşum hızının belirlenmesinin bir yolu olarak kullanılmıştır. Aynı zamanda, H_2S konsantrayonunun ve tuzluluğun metan-hidrojen sulfur hidratlarının oluşum koşulları üzerindeki etkisi çalışılmıştır. Tuzlulukta meydana gelen artışın metan-hidrojen sülfür hidrat denge koşulunu

belirli bir basınçta daha düşük denge sıcaklıklarına kaydırdığı gözlenmiştir. Ayrıca, H_2S konsantrasyonundaki artış ile birlikte metan-hidrojen sülfür hidratlarının oluşum koşullarının belirli bir basınçta daha yüksek denge sıcaklıklarına ulaştığı belirlenmiştir. Bu çalışma sonunda, yapılan deneylerin sonuçları değerlendirildiğinde Karadeniz'in metan hidrojen sülfür karışım hidratlarının oluşumu için uygun koşullara sahip olduğu sonucuna varılabilmektedir.

Keyword: Hidrat, Metan- Hidrojen Sülfür Karışımları, Hidrat Oluşum Koşulları, Karadeniz

To My Family

ACKNOWLEDGEMENTS

I would like to express my deep gratitude to my advisor Prof. Dr. Tanju MEHMETOĞLU for his help, support and supervision. I also would like to express my sincere gratitude to my co-Advisor Prof. Dr. Mahmut PARLAKTUNA for his support, encouragement, advice and guidance throughout the study. Without his valuable support, it would not be possible for me to gain my present knowledge of gas hydrates.

I would like to thank to Naci DOĞRU for his help and contribution during the experiments and in the construction of the experimental set-up.

I also would like to thank to Uğur KARABAKAL and Serhan TANRISINIBİLİR from the Turkish Petroleum Corporation (TPAO) Research Center and I would like to acknowledge the support provided by the Turkish Petroleum Corporation (TPAO) Research Center in the gas chromatography analysis of the gas samples used in the experiments. Also, I want to thank to Çağlar SINAYUÇ, Emine KAVDIR, Hale ÜÇKARDEŞ and Nevruz PARLAKTUNA for their valuble contribution during the study.

I also wish to thank to my friends, Çiğdem METİN, Emre ÖZGÜR and Mehmet SORGUN for their valuable support.

Finally, I would like to express my deepest gratitude to my family for being always beside me with their love, support and guidance throughout all my life and also throughout this study. Especially, I wish to thank to my nephew, Tuna for his new contribution to my life with love and joy, which makes easier all the difficulties I have encountered during my life and this study.

TABLE OF CONTENTS

LIST OF TABLES

LIST OF FIGURES

CHAPTER 1

INTRODUCTION

Gas hydrates are solid, crystalline compounds, which are composed of water and gas molecules. Hydrogen-bonded water molecules enclose gas molecules, forming a cage-like structure. The formation of gas hydrates are favored at the conditions of high pressure and low temperature.

The interest on gas hydrates has started with scientific researches, since there was not any industrial concern about gas hydrates previously. In 1810, Sir Humphrey Davy discovered gas hydrates, cooling chlorine gas and its aqueous solutions during his experimental studies. In 1934, Hammerschmidt recognized gas hydrates as the reason of the plugging problems in gas pipelines and gas hydrates were started to be considered as undesirable substances, which occur during oil and gas production and transportation activities. Finally, it was discovered that gas hydrates also exist in nature, in both deep oceans and permafrost regions [1, 2].

The study of gas hydrates has a very wide application, since gas hydrates can be considered as both useful and hazardous with different ways of consideration. It has been experienced many times that gas hydrates cause problems during oil and gas production and transportation operations by plugging transmission lines, causing pipeline blowouts and tubing, casing collapses, damaging equipment such as blowout preventers, heat exchangers, expanders and valves and complicating the construction of wells, off-shore platforms, and pipelines [3, 4]. Another concern about the gas hydrates is the possible effect of gas hydrates on global warming. Methane is the main component of most of the gas hydrates in nature and it is predicted that with methane hydrate dissociation and methane emission to the atmosphere, gas hydrates may play a significant role in global climate change in the future [4, 5].

Besides the disadvantages, some positive aspects of gas hydrates also exist. Gas hydrates are simply natural hydrocarbon resources and they may be considered as a future energy source. Gas hydrates have a huge potential of gas storage, namely, 1 ft^3 of hydrate may contain as much as 180 scf gas [3]. There exist many locations of gas hydrate occurences throughout the world, specifically, ocenic and permafrost regions, containing between a global amount of 10^{15} m^3 and 10^{17} m^3 methane in gas hydrates [6]. It is even predicted that the energy stored in gas hydrates equals nearly twice of all the world's other hydrocarbon sources [3]. Although there are uncertainities of gas hydrate evaluations and economical gas production strategies from gas hydrates, gas hydrates are still promising to be a new energy source [3] and even a way of natural gas storage and transportation, if the economical and technical conditions may be developed in the future for this purpose [7, 8].

In brief, gas hydrates are significant structures for both production and usage of oil and natural gas and for the future energy profile of the world. Consequently, further determinations and studies are required, in order to understand the properties of gas hydrates and to develop new technologies.

In this study, the main objective is to determine the hydrate formation conditions of methane- hydrogen sulfide mixtures. For this purpose, an experimental study has been carried out. During the experimental study, different hydrogen sulfide concentrations were considered and both distilled water and brine were used. Formation temperature and pressure values were obtained for the mixtures of methane and hydrogen sulfide.

CHAPTER 2

GAS HYDRATES

2.1. History of Gas Hydrates

It is widely accepted that gas hydrates were firstly obtained by Sir Humphrey Davy in 1810, although there were some observations of SO_2-hydrate by scientists; Pristley (1778), Bergman (1783), Fourcroy and Vauquelin (1796, 1798), Fourcroy (1801) before Davy [2]. After Davy's observation of chlorine hydrates, many scientists continued gas hydrate studies.

In 1823, Faraday determined the composition formula of chlorine hydrates. La Rive (1829), Pierre (1848), Schoenfeld (1855), Roozeboom (1884, 1885) and Schroeder (1927) carried out studies on SO_2 hydrates. In 1828, Löwig observed bromine hydrates and in 1876, Alexeyeff obtained the composition formula of Br_2 hydrates. Berthelot (1956), Millon (1960), Duclaux (1967) and Tanret (1978) determined the composition formula of the CS_2 hydrate. Chancel and Partemier (1885) observed chloroform hydrates, while Wroblewski (1882) studied about CO_2 hydrates. In 1877, Cailletet and Bordet made measurements on mixed gas hydrates. De Forcrand (1882-1925) studied H_2S hydrates and used Clasius- Claypeyron Equation to determine the composition of different hydrates, which was refined by Scheffer and Meyer in 1919. He also studied mixed hydrates of halohydrocarbons with Thomas and also obtained krypton and xenon hydrates. Villard (1888- 1896) continued studies on H_2S, CH_4, C_2H_6, C_2H_4, C_2H_2, C_3H_8, N_2O and Ar hydrates [1, 2].

In 1934, gas hydrates were initially recognized as the reason of the plugging problems in gas pipelines by Hammerschmidt. Hammerschmidt (1939), Deaton and Frost (1946), Bond and Russell (1949), Kobayashi et al. (1951) and Woolfolk (1952) studied the effects of inhibitors on gas hydrate formation. In 1945, Katz

developed a plot that can be used for estimating hydrate formation pressure values by using a given temperature and gas gravity. Deaton and Frost (1946) observed gas hydrates from pure components of methane, ethane and propane and also from their mixtures in natural gas. In 1941, Wilcox, Carson and Katz introduced the first analytic method for determining temperature and pressure values of hydrate formation from mixtures. Katz and co-workers (1959), Johari and Robinson (1965), Robinson and Ng (1976) and Poettman (1984) refined this study [1, 2].

In 1949-1958, von Stackelberg and co-workers used X-ray examinations and verified the theoretical information stated by Nikitin (1936- 1940), which explains the molecular cage-like structure of gas hydrates. von Stackelberg and Müller (1949, 1951, 1952), Claussen (1951), and Pauling and Marsh (1952) investigated that there exist two hydrate cyrstal structures and Dr. D. W. Davidson, S. A. Ripsmeester, J. S. Tse, V. P. Handa continued the studies on hydrate structures. Jeffrey and co-workers (1965, 1967, 1984) studied on each hydrate structure and determined gas hydrates to be in the class of clathrates [1,2].

In 1957, Barrer and Stuart developed a statistical thermodynamic approach to determine properties of gas hydrates and in 1959, van der Waals and Platteeuw proposed another method for predicting gas hydrate properties, which was refined by Child (1964), McCoy and Sinanoglu (1963), Marshall et al. (1964), Nagata and Kobayashi (1966), Parrish and Prausnitz (1972), Holder et al. (1988), Erbar et al. (1985), Anderson and Prausnitz (1986), Robinson et al. Sloan et al. (1987) [1, 2].
Gas hydrate kinetics were studied by Makogon and co-workers (1974, 1985) and gas hydrates were firstly considered as a promising natural energy source and initial proof of natural gas hydrates were extracted at the Ust-Viliuisk and Sredne-Viliuisk fields in Yakutiya and Messoyakha field in Western Siberia as stated by Makogon in 1972 [2]. Lubas (1978) and Bernard et al. (1979) recognized the hydrate formation in gas wells, while Bishnoi and co-workers investigated hydrate growth kinetics. Holder and co-workers and Sloan and co-workers also studied hydrate

kinetics [1]. In 1946, Strizhev stated the possibility of gas hydrate existence in natural geological conditions and Mokhnatkin (1947), Palvelev (1949) and Cherskiy continued these studies. In 1965, 1966, Y. F. Makogon indicated the possibility of gas hydrate formation in porous layers [1, 2]. In 1974, Miller stated that there exist CO_2 hydrates on Mars and in 1983, Pang et al. stated that the E-rings of Saturn were hydrates [1]. Delsemme and Miller (1970), Mendis (1974) and Makogon (1987) mentioned that there exist hydrates in comets and mentioned about the unusual locations of gas hydrate occurrence [1].

2.2. Structure of Gas Hydrates

Gas hydrates are solid inclusion compounds of water and gas molecules, which are the members of the class of compounds called "clathrates". The word "clathrate" originates from the Latin word "clathratus", which means "to encage" [1]. Hydrogen bonded water molecules, usually referred as "hosts" encage "guest" gas molecules and gas hydrates are formed at suitable temperature and pressure values. High pressure and low temperature values favor hydrate formation.

There exist five cavity structures (or polyhedra) that form the hydrate structure as indicated in Figure 2.1 [4]. 5^{12} indicates the cavity structure of pentagonal dodecahedra, which contains 12 faces of pentagonally bonded water molecules, while $5^{12}6^2$ indicates tetrakaidecahedron, containing 12 pentagonal and 2 hexagonal faces [1, 4]. Another cavity structure is the hexakaidecahedron, containing 12 pentagonal and 4 hexagonal faces ($5^{12}6^4$) [1]. The cavity structures formed by water molecules contain at most one guest molecule, which is held in the cage with van der Walls bonds [1]. There is no chemical bonding between the guest and host molecules of crystalline compounds of gas hydrates.

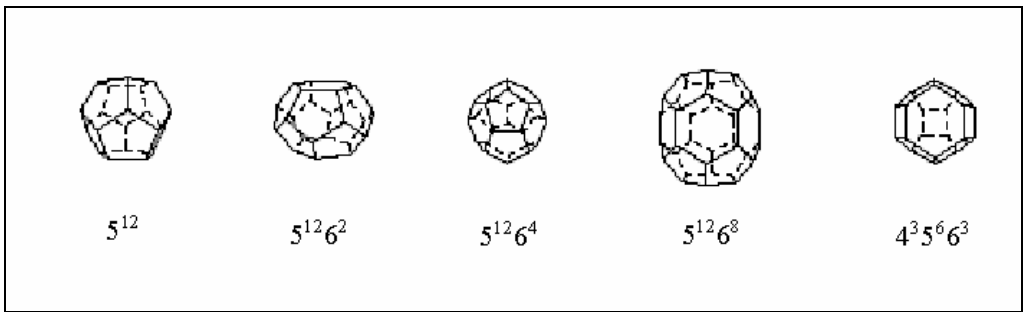

Figure 2.1- Cage Structures that Form Gas Hydrates [4]

The cavity structures are combined together to form 3 different hydrate structures, namely Sructure I, Structure II and Structure H hydrates. Structure I hydrates contain small guest molecules (0.4-0.55 nm) and composed of two 5^{12} and six $5^{12}6^2$ cavity structures with 46 water molecules [4]. 5^{12} cavity structures are attached to other 5^{12} blocks through the vertices in Structure I [4]. Structure I hydrates generally include small natural gas containing molecules smaller than propane, remaining in situ in deep oceans [9]. Methane, ethane and CO_2 are some of the formers of Structure I hydrates [4].

Structure II hydrates contain larger guest molecules of a range between 0.6-0.7 nm and are composed of sixteen 5^{12} and eight $5^{12}6^4$ cavity structures with 136 water molecules [4]. 5^{12} cavity structures are attached to other 5^{12} blocks through the faces in Structure II [4]. Structure II is a crystalline lattice within a cubic framework and generally formed from molecules larger than ethane, smaller than pentane [9]. Propane and isobutane are some of the formers of Structure II hydrates [4].

Until the discovery of Structure H hydrates by Ripmeester et al. in 1987, n-butane was considered to be the largest natural gas molecule forming hydrates [10, 11]. Ripmeester et al. reported the existence of a new type of hydrate structure, which may contain both large and small guest molecules [10]. Structure H hydrates are formed from the mixtures of both small and large guest molecules of 0.8-0.9 nm

[4]. They are composed of three 5^{12}, two $4^3 5^6 6^3$ and one $5^{12}6^8$ cavity structures with 34 water molecules [4]. The three 5^{12} and two $4^3 5^6 6^3$ have similar sizes, while the $5^{12}6^8$ cavity structure have a larger size applicable to hold large guest molecules [12]. For the stability, Structure H hydrates necessarily contain both small and large guest molecules [12]. The small cages of the structure are occupied by small guest molecules, referred as help gases (i.e. methane, H_2S, xenon) that increase the stability of the structure [12]. In Structure H hydrates, the connections of the cavity structures are obtained by a layer of linked 5^{12} cavities [9]. Methane + neohexane and methane + cycloheptane molecules are examples of guest molecules that can form Structure H hydrates [4]. The three different hydrate structures and their cavity structures are indicated in Figure 2.2 [4].

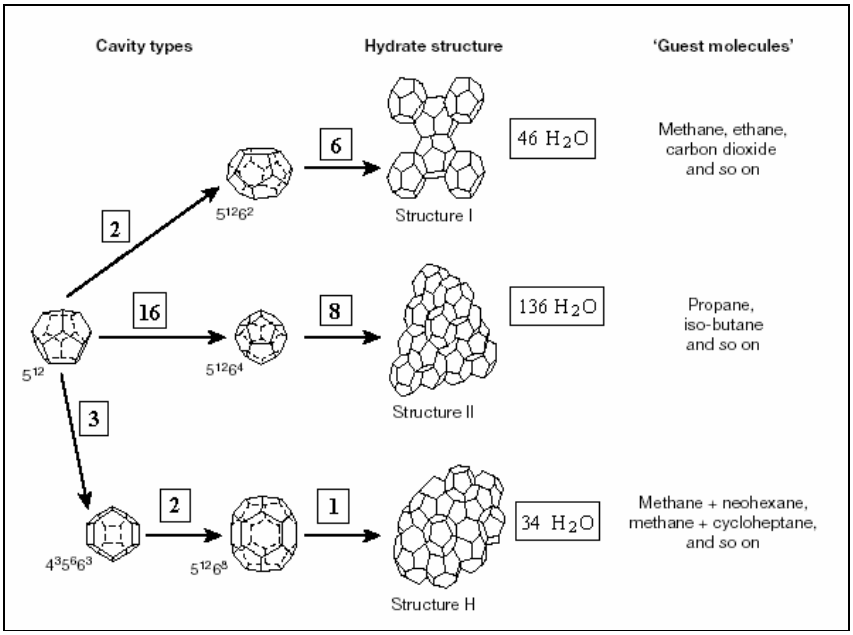

Figure 2.2- Different Hydrate Structures and Their Cavity Structures [4]

If all the cavities of each hydrate structures, Structure I, Structure II and Structure H are completely occupied with guest molecules, all of these hydrate structures have 85 mol % water and 15 mol % guest molecules [9]. The occupancy of the cavities of hydrate structures are dependent on the size ratio of the guest molecule to the cavities they enter [4]. Table 2.1 indicates the values of average cavity radius (A°) of hydrate structures [9]. Guest molecule sizes and their resultant hydrate structures are indicated in Figure 2.3, which is modified by Sloan Jr.[1] from the figure that was firstly developed by von Stackelberg [13]. The values on the line in Figure 2.3 demonstrates the sizes of the guest molecules. The number of water molecules occupied by the guest molecules are also indicated.

Some guest molecules can only occupy the large cavities of the structures, while the others can occupy both small and large cavities. For example, methane molecule is small enough to enter both the cavities of $5^{12}+ 5^{12}6^2$ in Structure I or $5^{12}+ 5^{12}\ 6^4$ in Structure II as a single guest molecule, as indicated in Figure 2.3 [9]. On the other hand, propane molecule is so large that it can only stabilize the largest cavity of Structure II, namely the cavity $5^{12}\ 6^4$ [4].

Table 2.1- The Values of Average Cavity Radius (A°) of Hydrate Structures [9]

	I		**II**		**H** (from geometric models)		
cavity	Small	Large	Small	Large	Small	Medium	Large
description	5^{12}	$5^{12}6^2$	5^{12}	$5^{12}6^4$	5^{12}	$4^3 5^6 6^3$	$5^{12}6^8$
average cavity radius (A°)	3.95	4.33	3.91	4.73	3.91	4.06	5.71

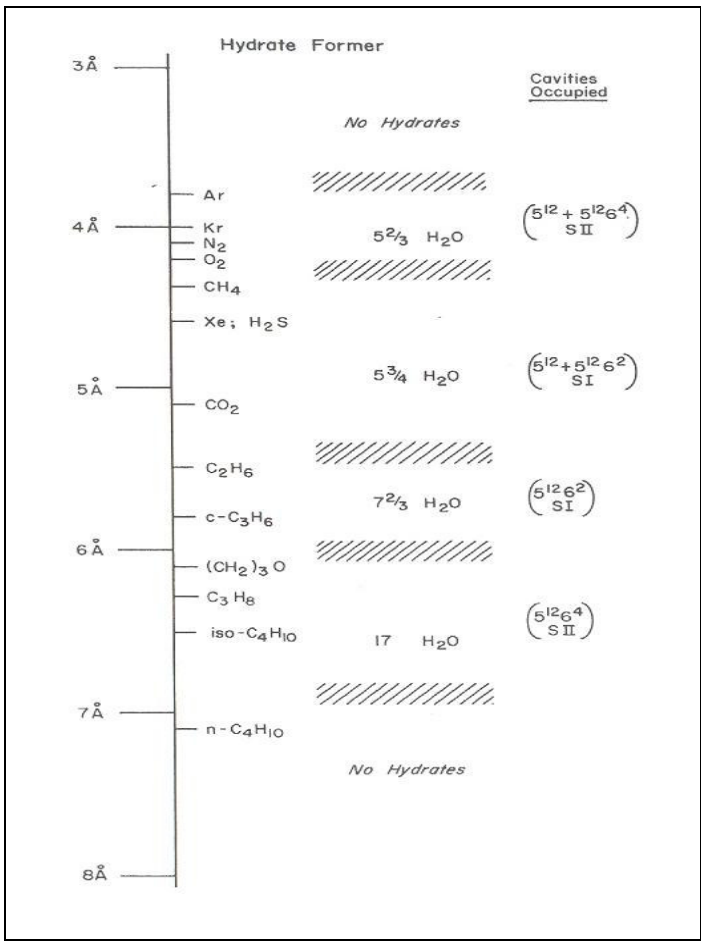

Figure 2.3- Guest Molecule Sizes And Their Hydrate Structures
(modified by Sloan, Jr. [1] from the figure developed by von Stackelberg [13])

2.3. Formation Conditions of Gas Hydrates

The formation of gas hydrates are directly dependent on the conditions of temperature and pressure, as well as the existence of water and at least one hydrate former. Phase diagrams of different natural gases that form hydrates are illustrated in Figure 2.4, which was modified by Sloan Jr. [1] from the plot developed by Katz [14]. In Figure 2.4, H is used for indicating hydrates, V for vapor, L_w for the aqueous liquid phase and L_{HC} for the hydrocarbon liquid phase. There are two

quadruple points, namely Q_1 (I- L_w- H- V), the lower hydrate quadruple point and Q_2 (L_w- H- V- L_{HC}), the upper quadruple point [1]. Q_1 shows the end of hydrate formation from vapor and liquid water and the beginning of hydrate formation from vapor and ice with decreasing temperature. On the other hand, Q_2 indicates the approximate intersection point of the line L_w- H- V with the vapor pressure of the hydrate former, presenting the upper temperature limit for hydrate formation [1].

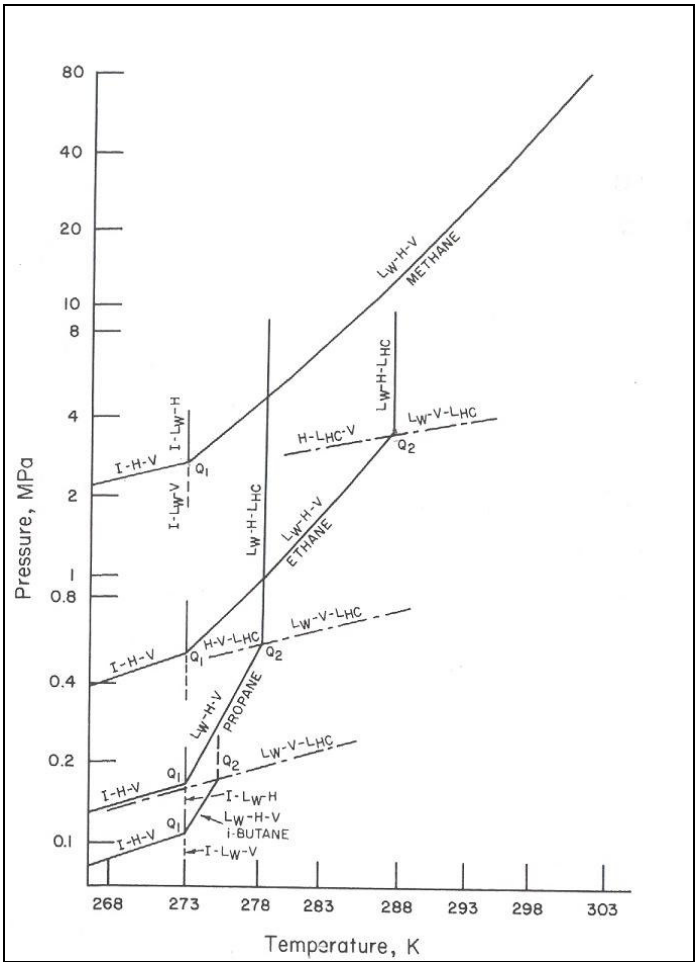

Figure 2.4- Phase Diagrams of Different Natural Gases that Form Hydrates (modified by Sloan Jr. [1] from the plot developed by Katz [14])

If there exist more than one component that form gas hydrates, the phase diagram slightly differs. Phase diagram of a multicomponent hydrocarbon mixture that form hydrates is presented in Figure 2.5, which is reproduced by Sloan Jr. [1] from the diagram of Robinson et al. [15]. The phase envelope of the gas mixture is represented by the curve ECFKL and it is superimposed on the hydrate formation line [1]. The upper quadratic point Q_2 in the single component system changes into the line $\overline{KC}$ in the multicomponent system in Figure 2.5 [1].

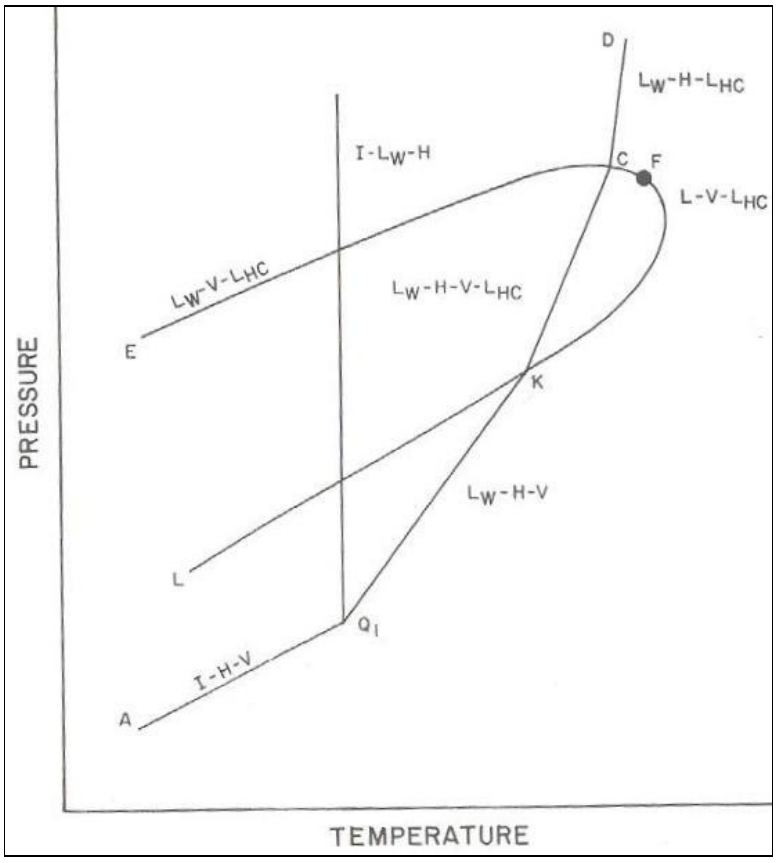

Figure 2.5- Phase Diagram of A Multicomponent Hydrocarbon Mixture that Form Hydrates (reproduced by Sloan Jr. [1] from the diagram of Robinson et al. [15])

CHAPTER 3

HYDRATES AS A POTENTIAL ENERGY SOURCE

Hydrates are considered to be one of the most promising energy sources that would meet the world's increasing energy demand in the future, with their huge potential of methane storage and worldwide geographical distribution [1, 2, 16, 17, 18, 19].

One of the main reasons of the prediction that gas hydrates are a potential energy source is that they have an extensive geographical distribution all over the world. Hydrates exist in many locations of the world; strictly, permafrost and ocenic regions, as a result of temperature and pressure requirements for hydrate formation. Sufficient amount of hydrate former gas molecules and water are required for hydrate formation as well as temperature and pressure values within the hydrate phase equilibrium region [2]. In continental polar regions, the upper depth limit is about 150 m below the surface, where the surface temperature value is below 0 °C for methane hydrates. On the other hand, in oceanic sediments, gas hydrate occurrence is at the water depths exceeding about 300 m, where bottom water temperature value approaches 0 °C [6].

Figure 3.1, indicates arbitrary examples of methane hydrate stability regions, respectively, in permafrost and in ocean sediments, which is reproduced by Sloan Jr. [1] from the figure of Kvenvolden [20]. The dashed lines indicate the thermal gradients as a function of depth, while the solid lines are plotted from methane hydrate phase equilibrium data by converting the pressure to depth assuming hydrostatic conditions [1]. The intersections of solid and dashed lines indicate the depths of the zone of hydrate formation. A hydrate formation zone (HFZ) can be described as a permeable, usually sedimentary rock with pressure and temperature conditions of a stable existence of hydrates [2]. The size of the hydrate formation

zone depends on the gas composition and salt content of formation water [2]. Gas hydrates, mostly the methane hydrates at the conditions of 1-2 to 50 MPa pressure and at 264-300 °K temperature values are considered as significant hydrate resources of interest [2].

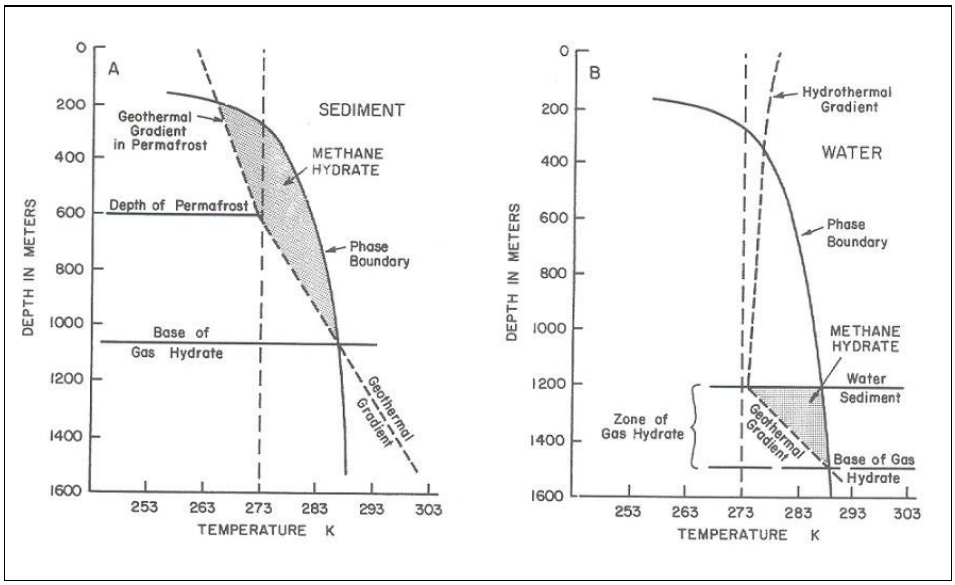

Figure 3.1- Methane Hydrate Stability Regions A) in Permafrost B) in Ocean Sediment (reproduced by Sloan Jr. [1] from the figure of Kvenvolden [20])

The hydrate occurrences are predicted and determined by data obtained from well drilling, well logging, seismic methods and core sampling in permafrost regions [1, 2]. Gas hydrate occurrences in oceans are interpreted by using seismic seafloor data. A region of strong reflection of sound waves, which is referred as bottom-simulating reflector (BSR), is determined [21]. BSR indicates the depth of hydrate occurrence at the bottom of the sea and is considered as the base of hydrate stability zone [6].

Locations of known and inferred gas hydrates exist all over the world in polar and oceanic outer continental margins, as indicated in Figure 3.2 [6]. The solid circles show gas hydrates in oceanic sediments; while the solid squares indicate the gas hydrates in permafrost regions. Gas hydrates in polar regions are encountered in permafrost regions both onshore in continental sediments and offshore in sediment of the polar continental shelves [6]. On the other hand, in oceanic outer continental margins, gas hydrates are encountered in sediment with cold bottom water, specifically, in the sediments of the continental slope and rise [6].

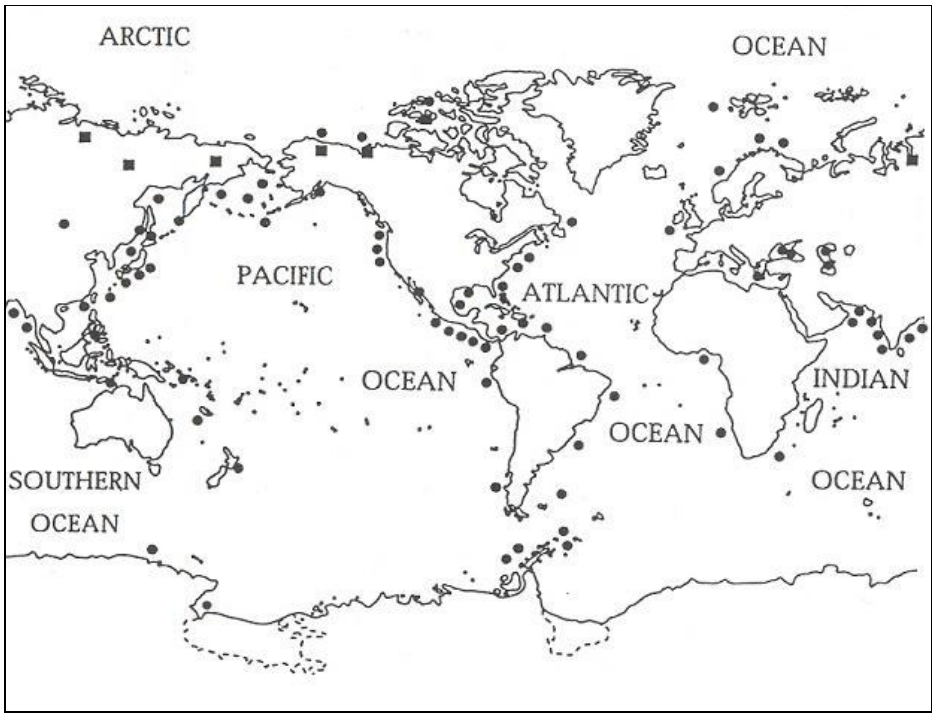

Figure 3.2- Locations of Known and Inferred Gas Hydrates in Oceanic Sediments (solid circles) and in Permafrost Regions (solid squares) [6]

From the time when gas hydrates were discovered on land in the Messoyakha field in Western Siberia, in the western Prudhoe Bay oil field in Alaska and in the Mackenzie Delta of Canada, nearly 20 oceanic hydrate occurrences have been identified. Some of the gas hydrate locations can be listed as offshore from Panama, Peru, Costa Rica, Guatemala, Japan, western and eastern United States, New Zealand, Russia, Argentina, Brazil, Norway, Oregon, California Gulf of Mexico, Black Sea, Caspian Sea, Sea of Okhotsk and Lake Baikal [2, 6].

Another reason why gas hydrates are considered to be a potential energy source is their huge gas storage capacities. The methane storage capacity of hydrates is 170 volumes of methane at standard conditions for one volume of methane hydrate [1]. As a result of this huge potential and the existence of many locations of hydrate occurrences through the world, it is expected that a large amount of fossil fuels of the earth is stored in hydrates. The amount of energy stored in hydrates is predicted to be twice of all the fossil fuels in the world [3].

Many studies were continued on the estimates of gas hydrates, suggesting the existence of a large methane content of gas hydrates [6]. After the study of Cherskiy and Makogon in 1970, the Potential Gas Committee proposed global gas hydrate estimates in a range of 3.1×10^{15} to 7600×10^{15} m^3 at standard conditions for oceanic sediments and in a range of 0.014×10^{15} to 34×10^{15} m^3 for permafrost regions in 1981 [6]. Between 1980 and 1990, better estimates were suggested and Kvenvolden and McDonald proposed a consensus value for the estimates of global gas hydrates, which is 21×10^{15} m^3 of methane [6]. In 1994, Gortniz and Fung stated estimates of a range between 26×10^{15} m^3 and 139×10^{15} m^3 and in 1995, Harvey and Huang calculated a value of 46×10^{15} m^3 as the ebst estimate of oceanic gas hydrates. Holbrook et al. (1996), Dickens et al. (1997), Makogon (1997) and Ginsburg and Soloviev (1995) proposed estimates smaller than the consensus value of 21×10^{15} m^3 [6]. It can be stated that the global estimate of gas hydrates is less than $\times 10^7$ m^3 and greater than 10^{15} m^3 by considering of previous studies [6].

CHAPTER 4

PROPERTIES OF THE BLACK SEA

The Black Sea is an inland sedimentary basin, located between the latitudes of 41 ° to 46 °N and longitudes of 28° to 41.5° E with an area of 423,000 km^2, a volume of 534,000 km^3 and a maximum depth of 2200 m [22]. It has a connection to the Sea of Azov by the Kerch Strait in the north, while it is connected to the Mediterranean Sea with the Bosphorus Strait through the Sea of Marmara in the south.

The Black Sea was a fresh water basin until the rise in the world sea level nearly 9000 years ago. As a result of the rise of the sea level to the sill depth of Bosphorous, an influx of the warm and saline waters was started from the Mediterranean Sea to the Black Sea. The denser saline water sank and replaced the bottom fresh water, spreading across the deep parts of the basin. This situation resulted in a density stratification that limits the transfer of the dissolved oxygen to the deep water and anoxic conditions started in the deepest parts of the basin [22, 23, 24, 25]. The anoxic depth of the Black Sea is at about 200 m [26].

The bottom water temperature values of the Black Sea are mentioned to be constant at a value of 9 °C after the depth of 250 m by Karabakal and Parlaktuna [27], with the consideration of the results of the International Project of TU- Black Sea Project in 1997 [28]. Poort [25] points out that the study of Vassilev and Dimitrov also indicates the bottom water temperatures to be slightly changing around 8.9 °C at a water depth more than 300 m with the consideration of data from 2320 different monitoring points in the Black Sea [29]. As a result of the International Project of TU- Black Sea Project [28], the salinity of seawater is indicated to be constant at 22 ppt, after the depth of 250 m in the Black Sea [27]. Figure 4.1 shows the water temperature and salinity changes in the Black Sea with depth [27, 28].

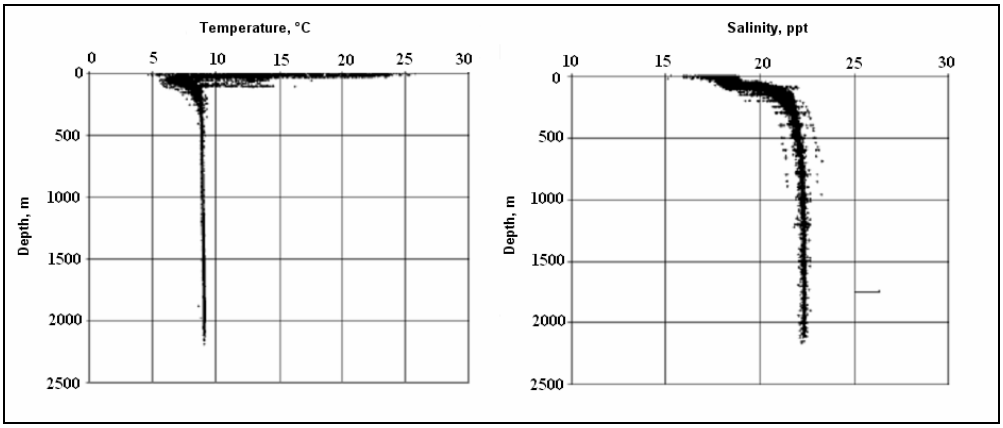

Figure 4.1- Water Temperature and Salinity Changes in the Black Sea with Depth [27, 28]

The Black Sea has an oxygen-hydrogen sulfide interface at the depths of 150-200 m [24]. It contains large amounts of organic matter as a result of being an inland sea with many rivers carrying organic compounds [26]. H_2S in the Black Sea is produced by the processes of bacterial sulfate reduction [30]. The concentration of H_2S increases with depth and after the depth of 1000 m; it reaches an average value of 300 μM [27, 28]. Figure 4.2 indicates changes of the H_2S concentration in the Black Sea with depth [27, 28].

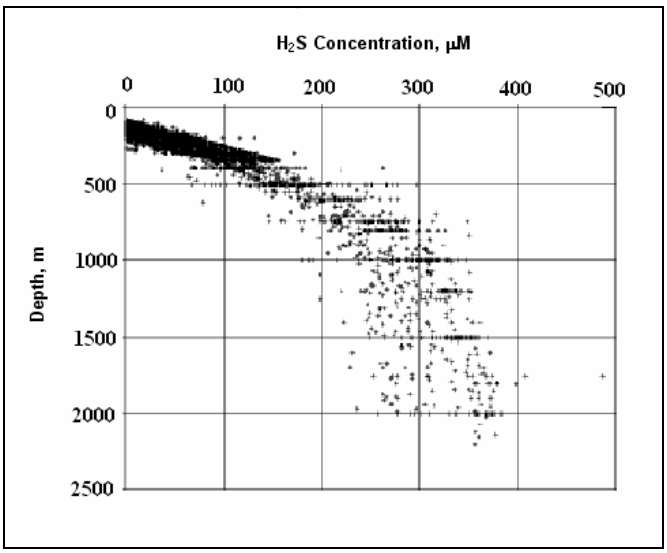

Figure 4.2- Changes of the H_2S concentration in the Black Sea with depth [27, 28].

Conditions of pressure and temperature in the Black Sea are appropriate for natural gas hydrate formation [2, 25, 27, 30]. Gas hydrate occurrences were investigated by using seismic indications and core sampling and five regions of hydrate deposits were determined in the Black Sea as it is shown in Figure 4.3 [2, 31].

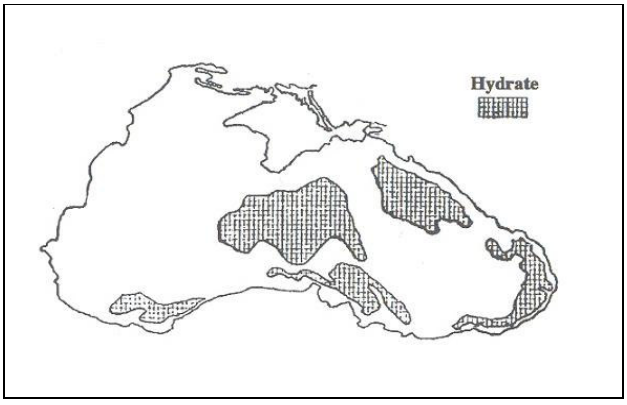

Figure 4.3- Gas Hydrate Occurrences in the Black Sea [2, 31]

Gas hydrates in the Black Sea mainly contain methane, which is produced due to the bacterial anaerobic reduction of CO_2 and fermentative transformations of organic matter in the sediments in the Black Sea [30]. Gas hydrate equilibrium conditions change with the components in the gas composition such as ethane, propane, carbon dioxide and hydrogen sulfide and the existence of H_2S results in higher equilibrium temperatures of methane hydrate formation at a given pressure [27, 32]. The Black Sea is favorable for hydrate formation with its H_2S containing environment starting from a depth of 200 m [27].

CHAPTER 5

FORMATION CONDITIONS OF METHANE HYDROGEN SULFIDE HYDRATES

The study of formation conditions of methane-hydrogen sulfide hydrates is an interest area of hydrates. Hydrogen sulfide, which is a common natural gas component, has strong tendency to form gas hydrates [33]. Noaker and Katz studied hydrate formation conditions of methane hydrogen sulfide mixtures experimentally and experimental data is plotted as shown in Figure 5.1 and Figure 5.2 [33].

In Figure 5.1, the hydrate formation conditions of the three component system containing methane, H_2S and water is presented. The equilibrium lines of methane-water and H_2S-water systems are labeled as 100 percent methane (0 percent H_2S) and 100 percent H_2S (0 percent methane). The lines placed between the lines of 100 percent methane and 100 percent H_2S show the conditions of the beginning of the hydrate formation at different H_2S compositions in the vapor phase, indicating the three phase equilibrium of water-rich liquid (L_1), hydrate (S) and vapor (V) [33]. After the point of 324.7 psia and 85.1 °F, the equilibrium line of S, L_1, V continues with another line indicated as (S)L_1(L_2)V with the appearance of the H_2S-rich liquid phase (L_2) [33].

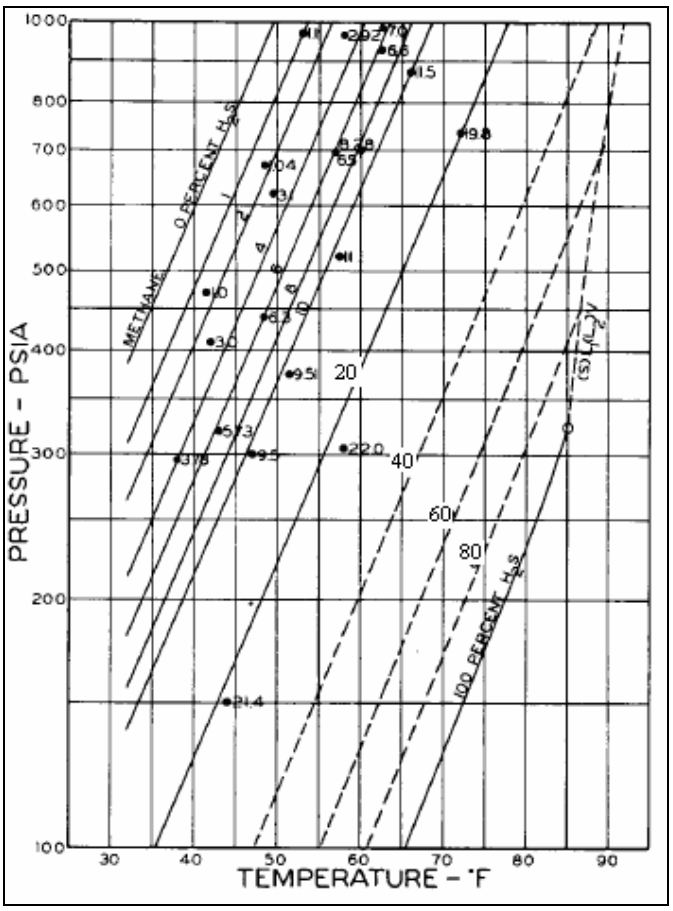

Figure 5.1- Formation Conditions of Methane H_2S Hydrate (P-T-mole % H_2S) [33]

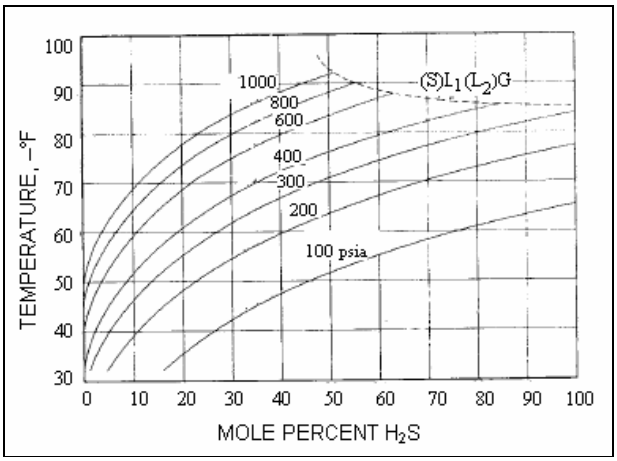

Figure 5.2- Formation Conditions of Methane H_2S Hydrate (T-mole % H_2S-P) [33]

The methane hydrate formation conditions reach higher equilibrium temperature values at a given pressure with the addition of H_2S [27, 32]. The change in the methane hydrate formation conditions as a result of different H_2S compositions are pointed out and the equilibrium curves are prepared by Karabakal and Parlaktuna [27] by the computer program of Colorado School of Mines Gas Hydrate Program (CSMHYD) [1], as shown in Figure 5.3. Another study of Kastner et al. [34] indicated the presence of methane H_2S hydrate at the Cascadia margin, offshore from central Oregon and determined the theoretical stability curves of the methane H_2S hydrate for 100 % methane and 90 % methane + 10 % H_2S mixtures, using Colorado School of Mines Gas Hydrate Program (CSMHYD) [1].

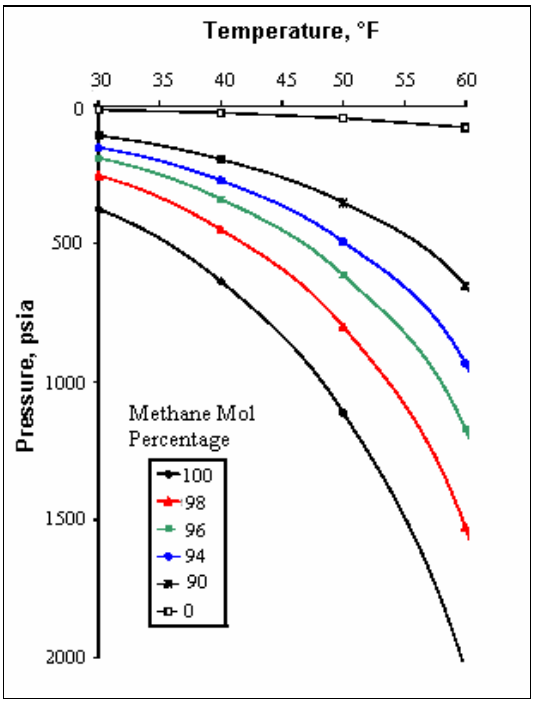

Figure 5.3- Hydrate Formation Equilibrium Curves of Methane H_2S Mixtures [27] (prepared by using the Colorado School of Mines Gas Hydrate Program (CSMHYD) [1])

CHAPTER 6

STATEMENT OF THE PROBLEM

Gas hydrates are structures that play a significant role on oil and gas production and also on the energy future of the world. As a potential energy source, gas hydrate formation conditions should be studied; in order to develop methods to use gas hydrates as an effective energy source in the future. The Black Sea, which has suitable conditions for the gas hydrate formation with its hydrogen sulfide containing environment, is a significant example of gas hydrate studies.

The main objective of this study is to investigate gas hydrate formation conditions of methane and hydrogen sulfide mixtures. For this purpose, an experimental study is carried out, considering the Black Sea conditions and hydrate equilibrium conditions are determined. The number of moles of free gas in the hydrate formation cell is also studied and the change in the number of moles of free gas with time is used as a way of determining the rate of hydrate formation. Effects of hydrogen sulfide concentration and salinity on the hydrate formation conditions are also obtained by using different H_2S concentrations and both brine and distilled water during the experiments.

CHAPTER 7

EXPERIMENTAL SETUP AND PROCEDURE

7.1. Experimental Setup

The experimental setup used to determine the formation conditions of methane-hydrogen sulfide hydrate is indicated in Figure 7.1.

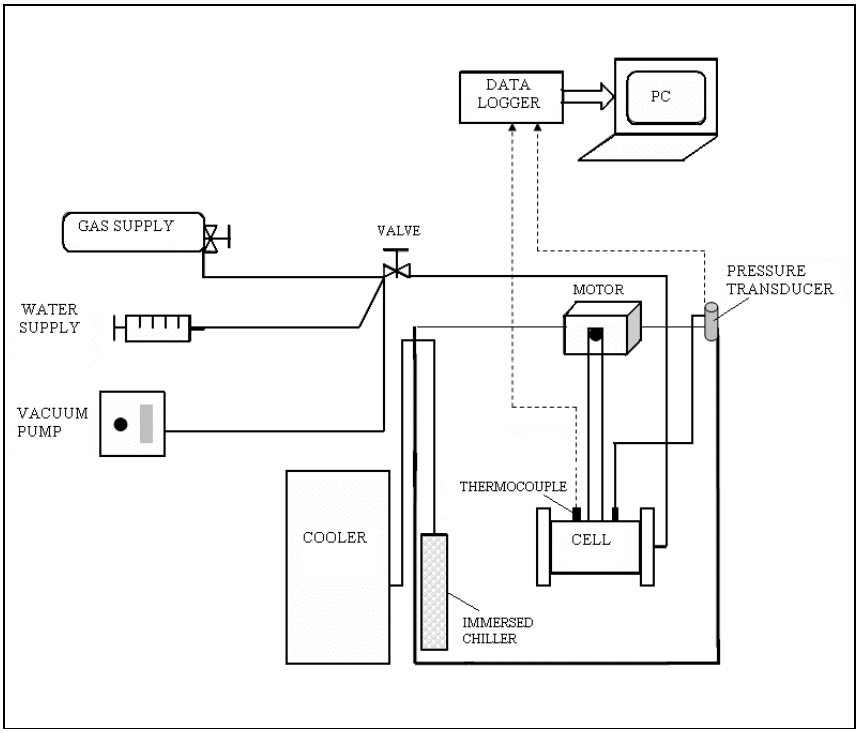

Figure 7.1- The Schematic Diagram of the Experimental Setup

The system contains a cylindrical high-pressure cell that has a volume of 600 cm^3, where the hydrate formation and dissociation processes develop, as indicated in Figure 7.2. The high-pressure cell is placed into a constant temperature water bath, which has a mechanism containing a motor for rocking the cell and a circulation system, as shown in Figure 7.3.

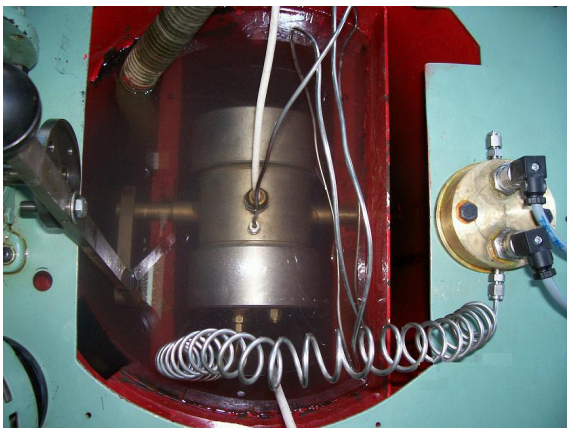

Figure 7.2- The High Pressure Cell of Hydrate Formation and Dissociation

Figure 7.3- Constant Temperature Water Bath with its Motor for Rocking

A refrigerated chiller is immersed into the water bath to control the cooling process. In order to determine the pressure and temperature values of the high-pressure cell, a pressure transducer and a thermocouple are connected to the cell and to the data logger. Another thermocouple is also added to the system to indicate the temperature values of the water bath. The data logger and a personal computer are used for recording temperature and pressure data in every 5 seconds. Glass marbles are placed into the cell to mix the cell components and to break the hydrate films for further growth of the hydrate.

A gas cylinder is used for preparing the methane- hydrogen sulfide mixture, which is tested for high pressures, as shown in Figure 7.4. The gas cylinder is filled with methane and hydrogen sulfide and used for charging the system, while syringes are used for charging water to the system. Valves and connection lines are added to make necessary connections from the high-pressure cell to the charge cylinder and to the pressure transducer. A vacuum pump is also a component of the system. Figure 7.5 and Figure 7.6 indicate the complete system of the experimental set-up. Specifications of the equipment used in the system are listed in Table 7.1.

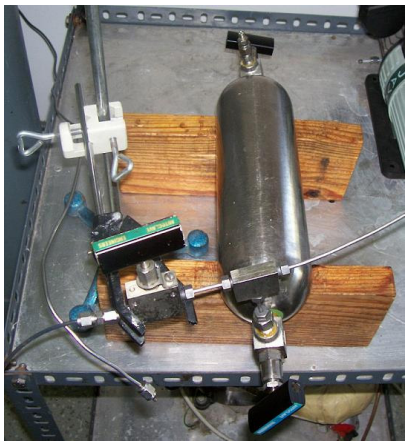

Figure 7.4- The Gas Cylinder Used for Gas Charging to the System

Figure 7.5- The System of the Experimental Set-up (with the connections to the charge cylinder)

Figure 7.6- The System of the Experimental Set-up

Table 7.1- Specifications of the Equipment Used in the Experimental Set-up

Pressure Transducer	
Trademark	GEMS Sensors, England
Model	1000BGC1001A3UA
Pressure Range	0- 100 bar G
Output	4- 20 mA
Supply	12 to 35 V
Precision	± 1 psig
Thermocouple	
Trademark	Elimko, Turkey
Model	PT- 100 (RT06- 1P06-4)
Temperature Range °C	-30 to + 40
Precision	± 0.2 °C
Data Logger and Controller	
Trademark	Elimko, Turkey
Model	E- 680- 08- 2- 0- 16-1-0
Voltage	220 V
Data Transfer	RS485 Mod Bus
Data Analysis	A package program of Elimko, Turkey

Table 7.1- Specifications of the Equipment Used in the Experimental Set-up (continued)

Immersed Chiller	
Trademark	PolyScience, USA
Model	KR- 50 A
Working Temperature	-30 to + 40 °C
Voltage	220 V/ 50 V
Immersion Probe Connection Length	100 cm Isolated metal pipe
Probe Diameter	$1^{1/2}$ in. / 3.8 cm
Compressor	1/ 4 HP
Watts at -30 °C	40
Watts at -20 °C	100
Watts at -10 °C	160
Watts at 0 °C	220
Watts at 10 °C	320
Watts at 20 °C	350
Cooling Capacity	Watts × 3.41= BTUs/ hr
Vacuum Pump	
Trademark	Javac, England
Model	DS40
Voltage	220 V/ 50 Hz
Type	Single stage high vacuum

7.2. Experimental Procedure

The experimental procedure consists of the following steps:

1. First of all, the methane- hydrogen sulfide mixture is prepared that will be used in the experiment. Hydrogen sulfide is firstly introduced to the evacuated gas cylinder, which will be used to charge the system, until the determined pressure value is reached and then the cylinder is filled with methane.

2. The high-pressure cell is placed into the water bath with glass marbles in it.

3. The next step is making the connections between the high-pressure cell and system components such as the pressure transducer and the gas transfer line. One of the thermocouple is placed into the water bath to indicate the temperature changes in the bath. The pressure transducer and thermocouple are also connected to the data logger for data recording.

4. After all the connections are made, air is injected to the system with the use of the needle valve controlling the gas flow to the cell, in order to check if there exist any leakage through the connections and through the high-pressure cell.

5. If it is observed that there is no leakage in the system, the high-pressure cell is evacuated.

6. After the evacuation, 300 ml distilled water or brine is injected into the cell.

7. Then, methane- hydrogen sulfide mixture is injected to the high-pressure cell until a different starting pressure value is reached for each experiment, by using the needle valve that controls the gas flow. While the gas mixture is introduced to the system, the gas charge cylinder is rocked for the complete mixing of the gas.

8. After the gas mixture is introduced to the system, rocking and cooling processes are started. The refrigerated chiller is immersed into the water bath and the system is cooled until the observation of the hydrate formation with a sharp decrease in the cell pressure.

9. When the rate of pressure decrease stabilizes, the refrigerated chiller is turned off. The temperature of the system begins to increase with the help of ambient temperature and the hydrate dissociation process starts.

10. Until the initial temperature and the pressure values of the system are reached, the temperature and pressure data is recorded.

11. Before starting another experiment, the system is heated until nearly 30°C, in order to prevent the tendency of forming hydrates more easily (memory effect of water) with the effect of the previous experiment.

12. The next experiment is started by adding methane-hydrogen sulfide mixture to the cell, until a pressure value higher than the previous experiment is reached. The procedure mentioned is repeated in each experiment.

CHAPTER 8

RESULTS AND DISCUSSION

In this study, hydrate formation conditions of methane hydrogen sulfide mixtures are investigated and the effects of change in H_2S concentration and salinity on the hydrate formation are examined. For this purpose, 25 experiments were carried out. During these experiments, three different gas mixtures having different methane hydrogen sulfide concentrations were used as hydrate forming gas phase. As a fourth group of experiments, pure methane was also used as hydrate forming gas. The concentration of hydrogen sulfide in the gas mixtures were measured by the gas chromatography at the Turkish Petroleum Corporation (TPAO) Research Center and the results for the each group of the experiments were reported to be 129, 86 and 62 ppm, respectively. The results of the gas chromatography, reported by TPAO Research Center are given in Appendix A.

The experiments are carried out with distilled and saline water. In the preparation of the saline water, the Black Sea conditions, which are suitable for hydrate formation with its hydrogen sulfide containing environment [27], are taken into consideration. The Black Sea water salinity is a constant value of 22 ppt after the depth of 250 m [27, 28]. In this respect, the saline water used in the experiments is prepared by adding 22 g NaCl to 1000 ml pure water (2 % wt NaCl) and mixing the solution with a magnetic stirrer.

According to the H_2S concentration and the water used in the experiments, experiments are classified into 4 groups. Table 8.1 indicates the classification of the experiments.

Table 8.1- Classification of the Experiments

(According to the H_2S Concentration and the Type of Water)

GROUP- I			
Experiment No	**H_2S Concentration (ppm)**	**Type of water**	**Initial Pressure at 15 °C (bar-g)**
I-1	129	Distilled water	37.98
I-2	129	Distilled water	43.07
I-3	129	Distilled water	51.32
I-4	129	Distilled water	51.22
I-5	129	Brine	35.14
I-6	129	Brine	39.55
GROUP- II			
Experiment No	**H_2S Concentration (ppm)**	**Type of water used**	**Initial Pressure at 12 °C (bar-g)**
II-1	86	Brine	34.00
II-2	86	Brine	38.78
II-3	86	Brine	45.90
II-4	86	Brine	51.78
II-5	86	Distilled water	34.31

Table 8.1- Classification of the Experiments
(According to the H_2S Concentration and the Type of Water) (continued)

GROUP- III			
Experiment No	**H_2S Concentration (ppm)**	**Type of water**	**Initial Pressure at 6 °C (bar-g)**
III-1	62	Brine	34.74
III-2	62	Brine	48.00
III-3	62	Brine	54.42
III-4	62	Brine	42.16
III-5	62	Distilled water	36.62
III-6	62	Distilled water	42.50
III-7	62	Distilled water	35.90
GROUP- IV			
Experiment No	**H_2S Concentration (ppm)**	**Type of water used**	**Initial Pressure at 10 °C (bar-g)**
IV-1	0	Distilled water	46.25
IV-2	0	Distilled water	52.32
IV-3	0	Brine	33.62
IV-4	0	Brine	47.67
IV-5	0	Brine	55.66
IV-6	0	Brine	55.66
IV-7	0	Brine	55.66

Experiments I-3 and I-4, IV-5, IV-6 and IV-7 were repeated under the same experimental conditions to see the reproducibility of the experiments. The results of reproducibility experiments will be discussed after introducing the sample plots obtained from each experiment.

In this experimental study, data of pressure-temperature vs. time, pressure vs. temperature and the number of free gas in the cell vs. time graphs are plotted for all experiments. In Figure 8.1, a typical hydrate formation and dissociation plot of pressure-temperature vs. time (Experiment II - 4) is presented. The pressure-temperature vs. time plots of all experiments are indicated in Appendix B.

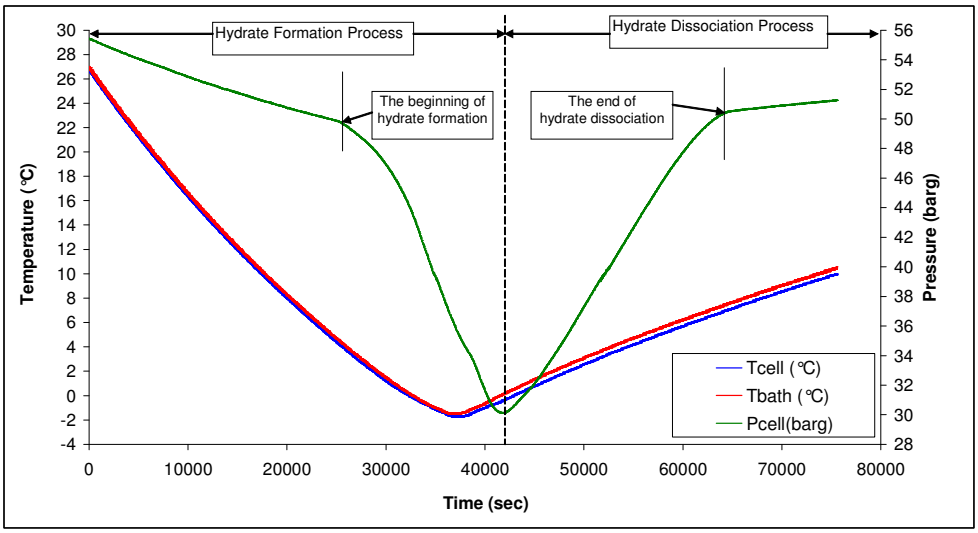

Figure 8.1- A Typical Hydrate Formation and Dissociation Plot of Pressure-Temperature- Time (Experiment II-4).

As it is indicated in Figure 8.1, initially, the system pressure drops gradually as a result of the cooling process, because of the relation between temperature and pressure as stated in the real gas law and since the solubility of free gas in water increases. Then, when hydrate formation begins, a sharp decrease in the pressure can be observed. This sudden change in the slope of the pressure curve is used to indicate the conditions of the beginning of hydrate formation. After the completion of hydrate formation process, the system is let to warm up with the help of ambient temperature and the hydrate dissociation process begins, resulting in an increase in the system pressure. In each experiment, hydrate formation and dissociation conditions are observed. The pressure- temperature vs. time plots of the experiments are indicated in Appendix B.

For each experiment, pressure vs. temperature plots of hydrate formation and dissociation is also constructed. Figure 8.2 shows a typical pressure vs. temperature plot of the hydrate formation and dissociation processes (Experiment II-4), namely the hydrate hysteresis. Hydrate formation and hydrate dissociation curves represent a complete cycle. The intersection point of the hydrate formation and dissociation curves is referred as the hydrate equilibrium point. In the literature, there are few explanations of the hydrate hysteresis of hydrate formation and dissociation. According to Schroeter and Kobayashi [36], the reason of the hysteresis is the metastability of hydrate forming compounds during the cooling portion. The supercooling effect usually causes a temperature difference in the equilibrium of the formation and dissociation [37] and the subcooling required to form enough critical nuclei for the initiation of hydrate formation is strongly affected by the extent of agitation [38].

The pressure vs. temperature plots of the experiments are presented in Appendix C. In all the experiments, the hydrate equilibrium points are observed, except from Experiment II-1 and Experiment II-2, in which some gas leakage resulted in a decrease in the cell pressure.

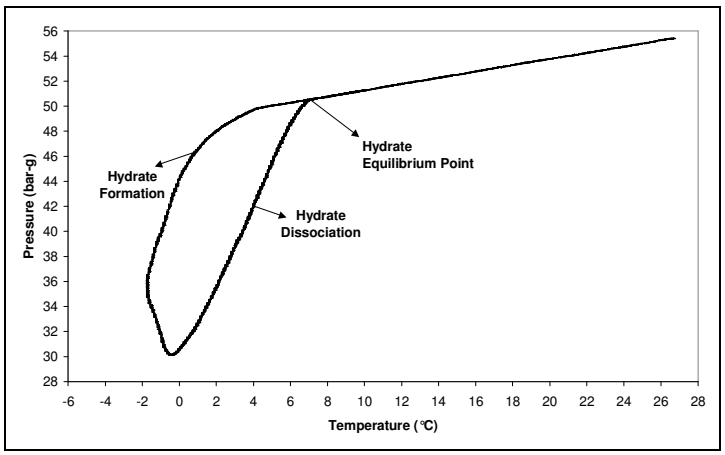

Figure 8.2- A Typical Hydrate Formation and Dissociation Plot of Pressure vs. Temperature (Experiment II-4)

Another result obtained from the experiments is the number of moles of free gas in the high-pressure cell. The number of free gas is obtained by using the computer program developed by Parlaktuna and Doğan [35]. The program calculates the number of moles of gas by using the real gas law expressed in Equation 8.1, determining the gas compressibility factor (z) at first. During the experiments, pressure and temperature values are recorded in every 5 seconds and the data recorded is used in the determination of number of moles of free gas in the cell. The volume of free gas in the cell is taken to be a constant value of 300 cm^3.

$$P\,V = z\,n\,R\,T \tag{8.1}$$

where

P: Cell pressure, psia

V: Volume of free gas in the cell, cuft

z: Gas compressibility factor

n: Number of moles of free gas in the cell, lb-mole

R: Universal gas constant, (10.73 psia cuft/ lb-mole °R)

T: Cell temperature, °R

In Figure 8.3, a typical number of moles of free gas- time plot is represented, which is plotted for Experiment II-4. As it is seen from the Figure, during the hydrate formation process, the number of moles of free gas in the cell decreases. After the hydrate dissociation process ends, the number of moles of free gas reaches its initial value.

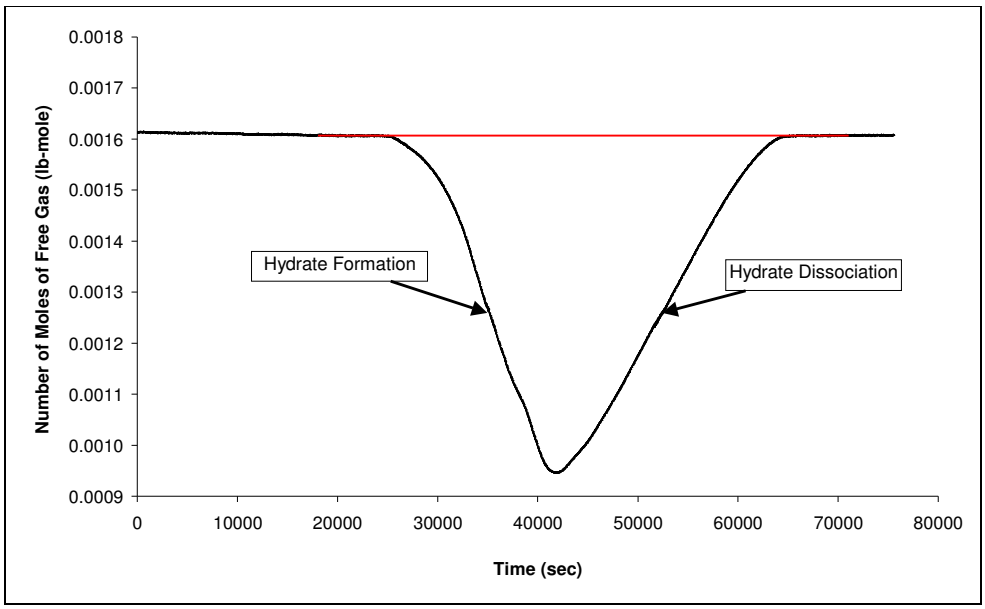

Figure 8.3- A Typical Number of Moles of Free Gas- Time Plot (Experiment II-4)

The change in the number of moles of free gas with respect to time indicates the rate of hydrate formation. The rate of hydrate formation can be determined by taking the derivative of the equation of the best line that fits the hydrate formation curve. In this study, first 1 hour period of the hydrate formation is considered to be the most representative period of all the experiments for the rate determination. It can be observed in Figure 8.4 that the equation of the best line that fits the hydrate formation curve in the first 1 hour period of hydrate formation can be written as

$n = -1.59819 \times 10^{-8}\, t + 2.01614 \times 10^{-3}$, where n is the number of moles of free gas in lb-mole and t is time in seconds. The derivative of the expression with respect to time indicates the rate of hydrate formation to be 1.59819×10^{-8} lb-mole/sec. The plots of the number of moles of hydrate formation vs. time data are represented in Appendix D.

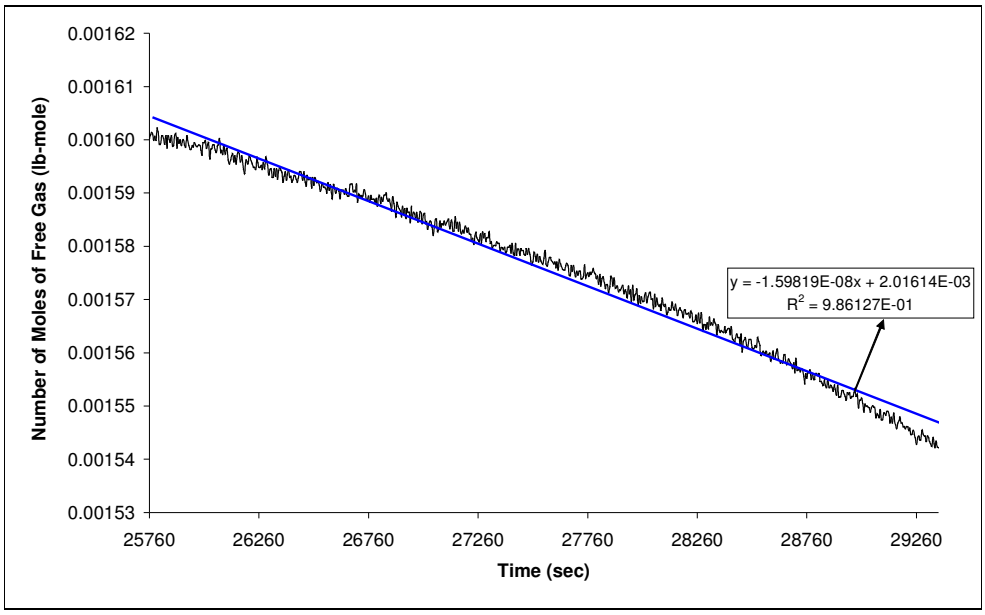

Figure 8.4- A Typical Number of Moles of Free Gas- Time Plot (Experiment II-4)

8.1 Repeatability

Experiments I-3, I-4 and IV-5, IV-6 and IV-7 are used to determine the repeatability of the experiments. In Figure 8.5, plots of the equilibrium pressure and temperature values of Experiment I-3 and I-4 are represented, in which distilled water and 129 ppm H_2S concentration is used. As it is shown in Figure 8.5, hydrate hysteresis curves of the two experiments are almost identical with a minor difference in hydrate equilibrium conditions. Furthermore, data of the other group of experiments of IV-5, IV-6 and IV-7 (0 ppm H_2S concentration, brine) show exactly the same results indicating repeatability of the experiments (Figure 8.6).

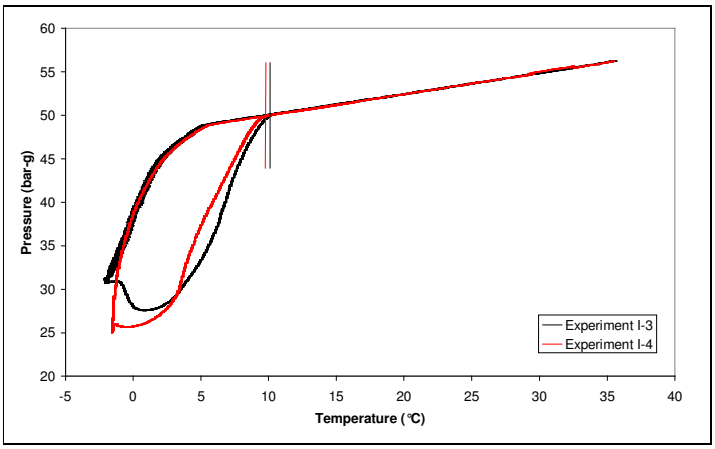

Figure 8.5- Pressure vs. Temperature Plots of Experiments I-3 and I-4

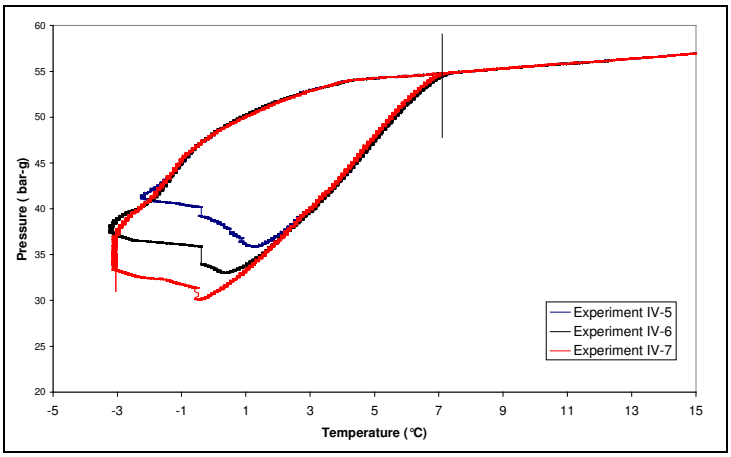

Figure 8.6- Pressure vs. Temperature Plots of Experiments IV-5, IV-6 and IV-7

8.2. Rate of Hydrate Formation

As it is mentioned previously, the change in number of moles of free gas with respect to time can be used to determine the hydrate formation rate. By deciding on that first 1 hour period of hydrate formation process of each experiment to be the most representative period for the determination of hydrate formation, hydrate formation rates are determined by taking the derivative of the equation of the best line that fits the hydrate formation process in the first 1 hour period. The hydrate formation rates and hydrate equilibrium pressure and temperatures are indicated in Table 8.2.

Table 8.2- Rate of Hydrate Formation and Equilibrium Pressure and Temperature Values of Experiments

Exp.	**Rate of Formation (lb- mole/ sec)**	**Initial Pres. at 15 °C (bar-g)**	**Equilibrium Temp. (°C)**	**Equilibrium Pres.(bar-g)**
I-1	1.5278×10^{-8}	37.98	7.12	36.42
I-2	1.3247×10^{-8}	43.07	8.11	41.56
I-3	2.0207×10^{-8}	51.32	10.18	50.08
I-4	1.8200×10^{-8}	51.22	9.79	49.97
I-5	1.0416×10^{-9}	35.14	7.42	33.91
I-6	1.2880×10^{-8}	39.55	8.70	38.56
Exp.	**Rate of Formation (lb- mole/ sec)**	**Initial Pres. at 12 °C (bar-g)**	**Equilibrium Temp. (°C)**	**Equilibrium Pres.(bar-g)**
II-1	1.5824×10^{-8}	34.00	2.08	29.37
II-2	1.3719×10^{-8}	38.78	3.96	35.68
II-3	1.8564×10^{-8}	45.90	5.94	44.40
II-4	1.5982×10^{-8}	51.78	7.12	50.54
II-5	1.1575×10^{-8}	34.31	3.66	32.86
Exp.	**Rate of Formation (lb- mole/ sec)**	**Initial Pres. at 6 °C (bar-g)**	**Equilibrium Temp. (°C)**	**Equilibrium Pres.(bar-g)**
III-1	4.1319×10^{-9}	34.74	3.37	34.22
III-2	1.6809×10^{-8}	48.00	6.43	48.05
III-3	1.4160×10^{-8}	54.42	7.62	54.93
III-4	1.0892×10^{-8}	42.16	5.24	42.01
III-5	1.4567×10^{-8}	36.62	4.26	36.23
III-6	1.7595×10^{-8}	42.50	5.54	42.40
III-7	1.4664×10^{-8}	35.90	4.06	35.50

Table 8.2- Rate of Hydrate Formation and Equilibrium Pressure and Temperature Values of Experiments (continued)

Exp.	Rate of Formation (lb- mole/ sec)	Initial Pressure at 10 °C (bar-g)	Equilibrium Temp. (°C)	Equilibrium Pres.(bar-g)
IV-1	1.5600×10^{-8}	46.25	5.84	45.34
IV-2	1.6586×10^{-8}	52.32	6.92	51.51
IV-3	1.1893×10^{-8}	33.62	2.68	32.40
IV-4	1.5446×10^{-8}	47.67	5.84	46.66
IV-5	1.9740×10^{-8}	55.66	7.32	54.85
IV-6	1.6286×10^{-8}	55.66	7.32	54.85
IV-7	2.0356×10^{-8}	55.66	7.32	54.95

In Figure 8.7- Figure 8.10, the relationship between the hydrate formation rates and equilibrium pressure values are plotted for H_2S concentrations of 129 ppm, 86 ppm, 62 ppm and 0 ppm, respectively.

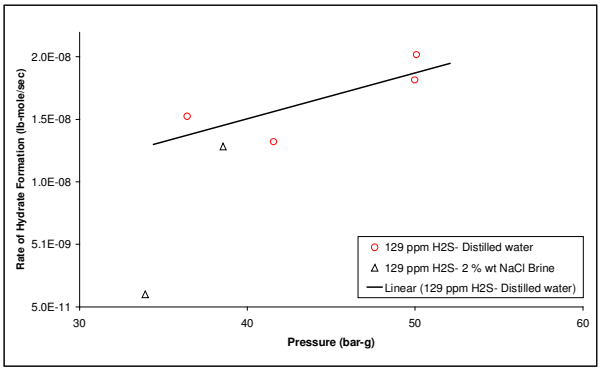

Figure 8.7- Hydrate Formation Rate vs. Equilibrium Pressure (Group I)

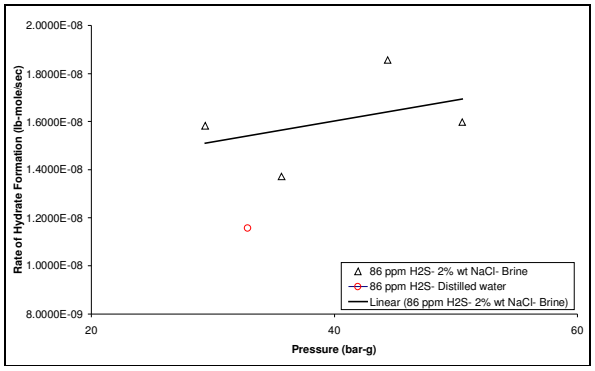

Figure 8.8- Hydrate Formation Rate vs. Equilibrium Pressure (Group II)

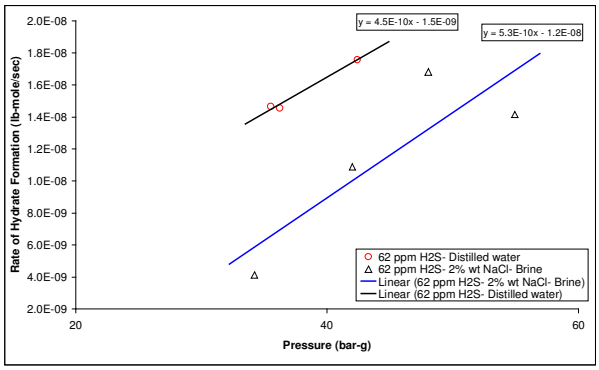

Figure 8.9- Hydrate Formation Rate vs. Equilibrium Pressure (Group III)

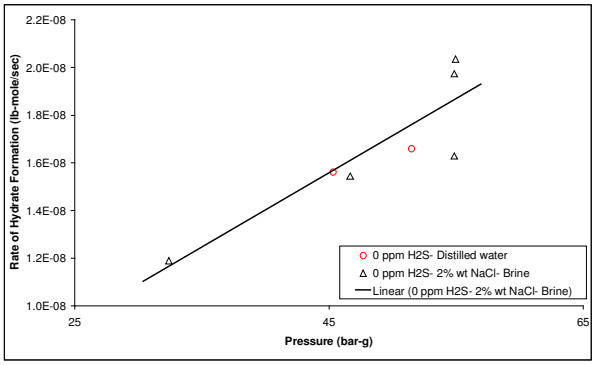

Figure 8.10- Hydrate Formation Rate vs. Equilibrium Pressure (Group IV)

All plots indicate a common behavior that there is an increase in hydrate formation rate with the increase in the hydrate equilibrium pressure. Although there exist some scatter in the absolute values of hydrate formation rates with equilibrium pressure, the change in hydrate formation rate can be expressed as a linear function of hydrate equilibrium pressure.

8.3. Hydrate Equilibrium Conditions

One of the main objectives of the experimental study is to obtain the methane-hydrogen sulfide hydrate equilibrium conditions and the effects of H_2S concentration and salinity on the equilibrium conditions. Hydrate equilibrium points are obtained from hydrate formation-dissociation experiments as the intersection point of formation and dissociation curves (Figure 8.2). Data of equilibrium temperatures and pressures are obtained for the experiments of distilled water and brine with 129 ppm, 86 ppm, 62 ppm and 0 ppm H_2S concentration and presented in Table 8.2.

In Figure 8.11, the Cartesian plot of equilibrium pressure and temperature values for the experiments conducted with distilled water and brine with 129 ppm H_2S concentration is presented. As it is known from the literature, hydrate equilibrium temperature is related to the hydrate equilibrium pressure exponentially. This knowledge was applied to the plot in Figure 8.11 resulted with an exponential fit of data having the regression coefficient of 0.9843 (very close to 1) which indicates a satisfactory fit. As a result, all the data of the other experiments are also represented in semi-log plots in Figure 8.12- Figure 8.15 and a linear relationship between hydrate equilibrium temperatures and pressures is observed.

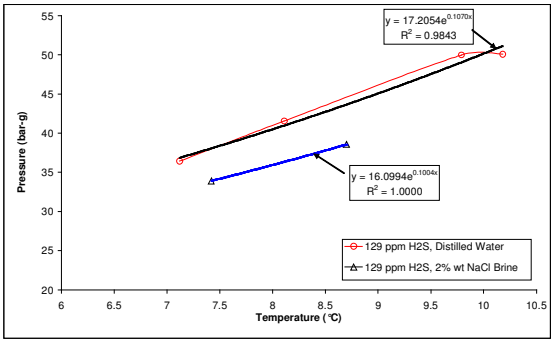

Figure 8.11- Hydrate Equilibrium Pressure vs. Temperatures (Group I)

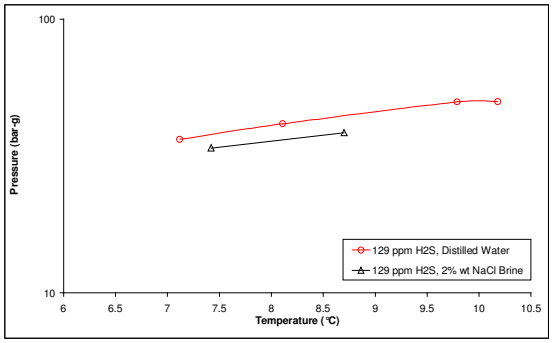

Figure 8.12- Semi-log Plot of Hydrate Equilibrium Pressure vs. Temperatures (Group I)

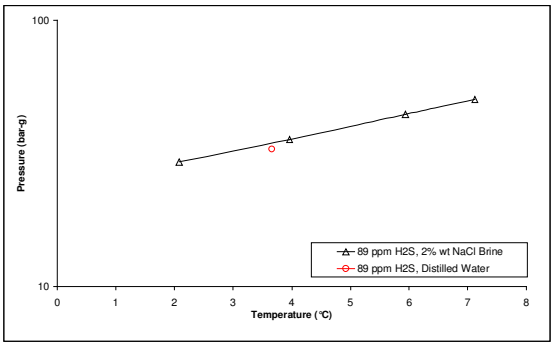

Figure 8.13- Hydrate Equilibrium Pressure vs. Temperatures (Group II)

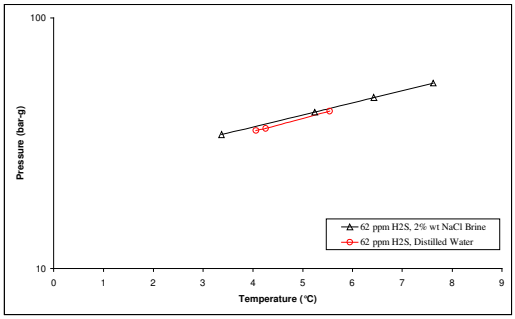

Figure 8.14- Hydrate Equilibrium Pressure vs. Temperatures (Group III)

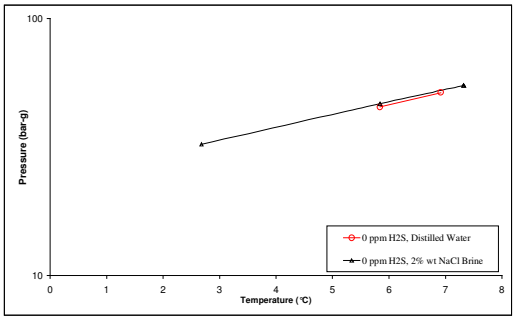

Figure 8.15- Hydrate Equilibrium Pressure vs. Temperatures (Group IV)

In Figure 8.11, equilibrium pressure and temperature values of Experiment Group-I (129 ppm H_2S concentration) are indicated. The data show that the equilibrium temperature and pressure values are directly proportional. However, the expected effect of salinity on hydrate equilibrium conditions could not be observed. It is expected that an increase in salinity should shift the methane-hydrogen sulfide hydrate equilibrium condition to higher equilibrium pressures for a given temperature [1, 32]. One of the reasons of the unexpected result obtained from this group of experiments can be predicted to be the gas charging process during the preparation of the experiments. As it was mentioned before, during the gas charging, the gas cylinder was rocked continuously to obtain a uniform gas composition transfer from the gas charging cylinder to the hydrate formation cell. It

could be possible to have insufficient shaking and mixing of the gas content of the gas charging cylinder during the preparation of this group of experiments and it may cause a higher H_2S concentration because of the nonuniform gas content distribution. Consequently, effects of H_2S concentration and salinity on hydrate formation may be cancelled out each other and the expected effect of the salinity may not be observed.

It can be observed from Figure 8.13, Figure 8.14 and Figure 8.15 that salinity has an inverse effect on hydrate formation and an increase in the salinity shifts the methane-hydrogen sulfide hydrate equilibrium condition to lower equilibrium temperatures at a given pressure. Higher hydrate equilibrium temperatures are obtained from the experiments carried out with distilled water than the experiments carried out with brine.

The effect of H_2S concentration is also considered during the study. In Figure 8.16 and Figure 8.17, hydrate equilibrium temperature and pressure values are plotted for the experiments carried out with brine and distilled water.

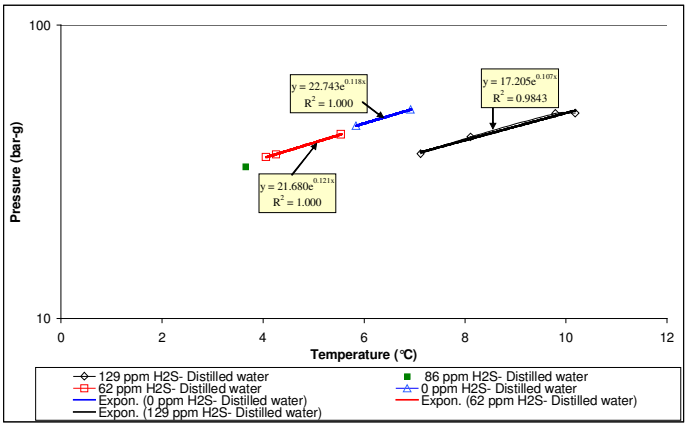

Figure 8.16- Hydrate Equilibrium Pressure vs. Temperatures-Distilled Water

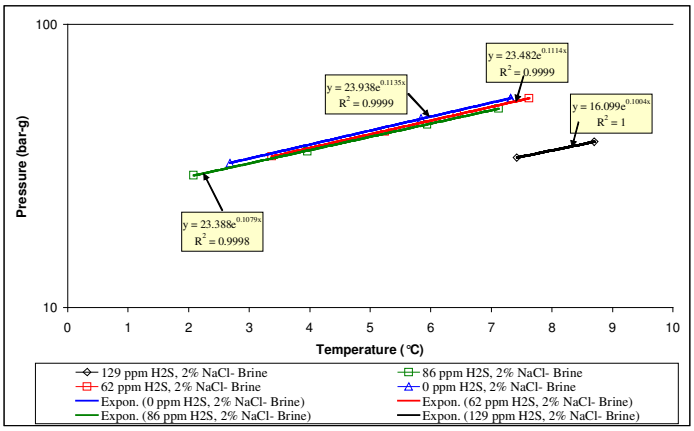

Figure 8.17- Hydrate Equilibrium Pressure vs. Temperatures- Brine

As it can be observed from the Figure 8.16 and Figure 8.17, the methane-hydrogen sulfide hydrate formation conditions reach higher equilibrium temperature values at a given pressure with the increase in the H_2S concentration. The higher the H_2S concentration is, the higher the hydrate equilibrium temperature at a given pressure for both distilled water and brine.

Considering the results of the experiments, the following expression can be stated to indicate the relationship between hydrate equilibrium pressure and temperature:

$$\log P_e = A\, e^{B T_e} \tag{8.1}$$

where

P_e: Hydrate equilibrium pressure, bar-g

T_e: Hydrate equilibrium temperature, °C

A, B: Equilibrium constants

In Table 8.3, the equilibrium constants for different H_2S concentrations and for both distilled water and brine is listed, by considering the experimental data obtained.

Table 8.3- The Equilibrium Constants for Different H_2S Concentrations and Distilled Water and Brine

Distilled Water		
H_2S Concentration (ppm)	**A**	**B**
0	22.744	0.118
62	21.680	0.121
129	17.205	0.107
Brine (2 % wt NaCl)		
H_2S Concentration (ppm)	**A**	**B**
0	23.938	0.1130
62	23.482	0.1140
86	23.388	0.1079
129	16.099	0.1004

Hydrate equilibrium temperature and pressure data obtained from the experiments are compared with hydrate equilibrium conditions that are determined using the computer program CSMHYD [1] and indicated in Figure 8.18 and Figure 8.19 for both distilled water and brine.

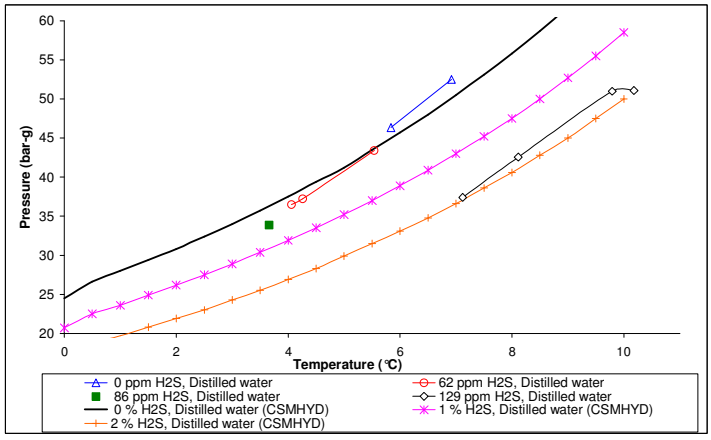

Figure 8.18- Comparison of Experimental Data with the Results of CSMHYD [1] Distilled Water

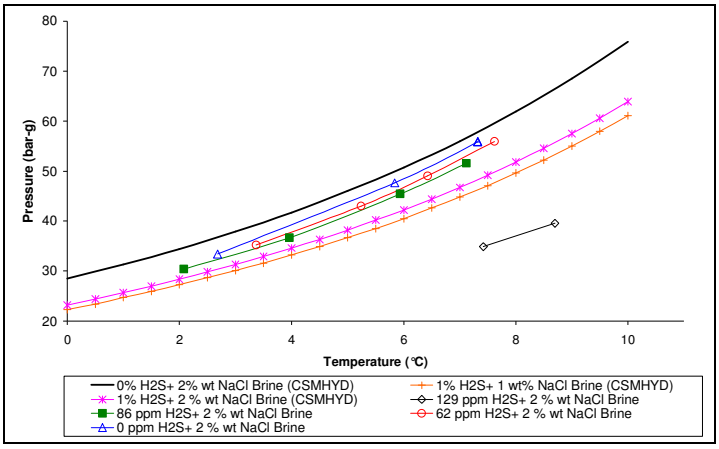

Figure 8.19- Comparison of Experimental Data with the Results of CSMHYD [1] Brine

In Figure 8.18 and Figure 8.19, it can be observed that hydrate equilibrium temperature and pressure data obtained from the experiments follow almost the same trend with the results of CSMHYD [1]. Although the data of the experiments are close to the results of CSMHYD, the data of Experiment Group-I for 129 ppm H_2S, especially for brine differ from the results of CSMHYD [1]. For a better comparison between the results, unit conversion from parts per million (ppm) to mole per cent for 129, 86 and 62 ppm H_2S concentration is included in Appendix E, which is determined using the results of gas chromatography reported by Turkish Petroleum Corporation (TPAO). It is calculated that 129 ppm H_2S concentration corresponds to 0.0064 % mole H_2S, while 86 ppm and 62 ppm H_2S concentration are calculated to be 0.0041 % mole H_2S and 0.0030 % mole H_2S, respectively. The H_2S concentrations used in the experiments are very close to 0 % mole H_2S as it is seen in Figure 8.18 and 8.19, except from Experiment Group I. It can be stated that although the common behavior of the experimental results with the results of CSMHYD is observed, a quantitative comparison between the results is not possible due to very low H_2S concentration in experimental part of this study.

8.4. Black Sea Hydrate Formation Conditions

Results of the experiments are analyzed to determine if the Black Sea has suitable conditions for methane-hydrogen sulfide hydrate formation. During the experiments, the Black Sea salinity condition is provided (2% wt NaCl). Equilibrium temperature and pressure data obtained from the experiments and Black Sea temperature and pressure values [27] are plotted by converting the pressure data to depth, as shown in Figure 8.20. Results of the computer program CSMHYD [1] for 0 % and 2 % H_2S concentration and 2 % wt NaCl Brine are also included in Figure 8.20.

From the intersection points of extrapolated hydrate equilibrium curves of experimental results and the curve of the Black Sea conditions, hydrate formation depths are determined for 129, 86, 62 and 0 ppm H_2S concentrations. As shown in Figure 8.20, the Black Sea has suitable conditions for methane hydrogen sulfide mixtures at a minimum depth of 400 m for 129 ppm H_2S concentration. For 86, 62 and 0 ppm H_2S concentrations, the Black Sea has appropriate conditions at the depths of 613, 625, 663 m and deeper, respectively. As the H_2S concentration increases, the minimum depth of hydrate formation of methane-hydrogen sulfide mixtures decreases. By considering the results of the experiments, it can be stated that the Black Sea has suitable conditions for hydrate formation of methane hydrogen sulfide mixtures.

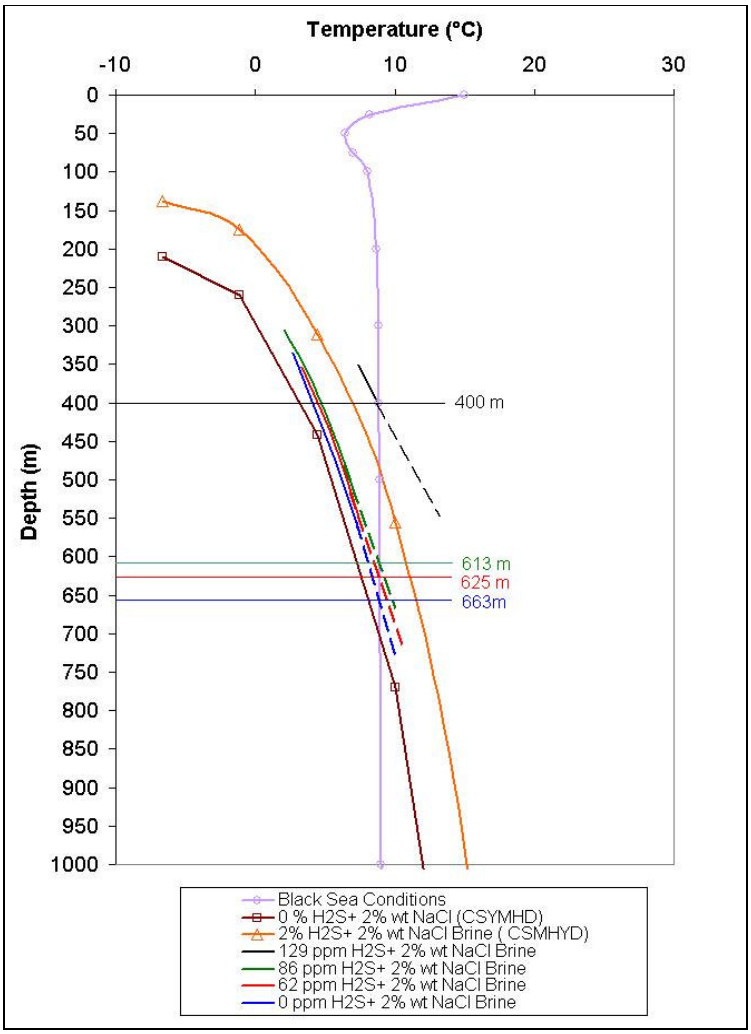

Figure 8.20- Black Sea Hydrate Formation Conditions for 129, 86, 62 and 0 ppm H_2S Concentration

CONCLUSION

In this study, an experimental work is carried out to obtain the hydrate formation conditions of methane-hydrogen sulfide mixtures. Hydrate equilibrium conditions are determined as well as the number of moles of free gas in the hydrate formation cell and rate of hydrate formation. During the experiments, pressure- temperature-time, pressure- time and the number of moles of free gas-time data are analyzed and the following results are obtained:

- There is an increase in hydrate formation rate with the increase in the hydrate equilibrium pressure. The change in hydrate formation rate can be expressed as a linear function of hydrate equilibrium pressure.

- Salinity has an inverse effect on hydrate formation. An increase in the salinity shifts the methane-hydrogen sulfide hydrate equilibrium condition to lower equilibrium temperatures at a given pressure.

- With an increase in the H_2S concentration, the methane hydrogen sulfide hydrate formation conditions reach higher equilibrium temperature values at a given pressure.

- Considering the results of the experiments, it can be stated that the Black Sea has suitable conditions for hydrate formation of methane hydrogen sulfide mixtures.

- As the H_2S concentration increases, the minimum depth of hydrate formation of methane-hydrogen sulfide mixtures decreases.

REFERENCES

[1] Sloan, E. D. Jr.: *Clathrate Hydrates of Natural Gases*, Marcel Dekker, Inc., New York (1990), 641 pp.

[2] Makogon, Y. F.: *Hydrates of Hydrocarbons*, Pennwell Books, Tulsa (1997), 482 pp.

[3] Sloan, E. D. Jr.: "Natural Gas Hydrates", *JPT* (December 1991), *SPE Technology Today Series*, SPE 23562, 1414-1417.

[4] Sloan, E. D. Jr.: " Fundamental Principles and Applications of Natural Gas Hydrates", *Nature* (2003), Vol. 426, 353-359.

[5] Haq, B. U.: "Climatic Impact of Natural Gas Hydrate", in *Natural Gas Hydrate- in Ocenic and Permafrost Environments*, D. M. Max, ed., Kluwer Academic Publishers, Netherlands (2003), 137-148.

[6] Kvenvolden, K. A.: " Natural Gas Hydrate: Background and History of Discovery", *in Natural Gas Hydrate- in Ocenic and Permafrost Environments*, D. M. Max, ed., Kluwer Academic Publishers, Netherlands (2003), 9-16.

[7] Gudmundsson, J. S., Parlaktuna M. and Khokhar, A.A.: " Storage of Natural Gas as Frozen Hydrate", *SPE Production and Facilities*, (February 1994), 69-73.

[8] Shirota, H. et al.: "Measurement of Methane Hydrate Dissociation for Application to Natural Gas Storage and Transportation", *Proc. 4th Int.Conf. Gas Hydrates* (2002).

[9] Sloan, E. D. Jr.: "Gas Hydrates: Review of Physical/ Chemical Properties", *Energy& Fuels* (1998), 12, 191-196.

[10] Ripmeester, A. J. et al. : "A New Clathrate Hydrate Structure", *Nature* (January 1987), Vol. 325, 135-136.

[11] Khokhar, A. A., Gudmundsson, J. S. and Sloan E. D.: "Gas Storage in Structure H Hydrates", *Fluid Phase Equilibria* (1998), 150-151, 383-392.

[12] Mehta, A. P. and Sloan, E. D.: "Structure H Hydrates: Implications for the Petroleum Industry", *SPE Journal* (March 1999), Vol. 4, No.1, 3-8.

[13] von Stackelberg M., *Naturwiss* (1949), 36, 327-359.

[14] Katz et al.: "*Handbook of Natural Gas Engineering"*, McGraw- Hill, New York (1959), 809 pp.

[15] Robinson, D. B., *Proc. 66th, Annual GPA Convention* (March 16- 18, 1987), Denver, CO.

[16] Makogon, Y. F: "Gas Hydrates as a Resource and Mechanism for Transmission", paper SPE 77334, prepared for presentation at *the SPE Annual Technical Conference and Exhibition* in San Antonio, Texas, 29 September-2 October 2002.

[17] Gupta, A. K.: "Marine Gas Hydrates: Their Economic and Environmental Importance", *Current Science* (10 May 2004), Vol. 86, No. 9, 1198-1199.

[18] Collett, T. S.: "Natural Gas Hydrates as a Potential Energy Resource", in Natural Gas Hydrate- *in Ocenic and Permafrost Environments*, D. M. Max, ed., Kluwer Academic Publishers, Netherlands (2003), 123-136.

[19] Max, M. D.: "Hydrate as a Future Energy Resource for Japan", in Natural Gas Hydrate- *in Ocenic and Permafrost Environments*, D. M. Max, ed., Kluwer Academic Publishers, Netherlands (2003), 225-238.

[20] Kvelvolden, K. A.: "Methane Hydrate- A Major Reservoir of Carbon in the Shallow Geosphere", *Chemical Geology* (1988a), 71, 41-51.

[21] Klauda, B. J., Sandler, I. S.: "Predictions of Gas Hydrate Phase Equilibria and Amounts in Natural Sediment Porous Media", *Marine and Petroleum Geology* (2003), 20, 459-470.

[22] Oğuz, T. et al.: "Physical and Biogeochemical Characteristics of the Black Sea", in *The Sea*, Robinson, R. A and Brink. K., ed., Harvard University Press (2005), Vol. 14B, the Global Coastal Ocean, Interdisciplinary Studies and Syntheses, Chapter 33, 1331-1369.

[23] Deuser, W. G. : "Evolution of Anoxic Conditions in Black Sea During Holocene", in *The Black Sea-Geology, Chemistry, and Biology*, Degens, E. T. and Ross, A. D., ed., The American Association of Petroleum Geologists, United States (1974), 133-136.

[24] Baykara, S. Z. et al.: " Hydrogen From Hydrogen Sulphide in Black Sea", *International Journal of Hydrogen Energy* (2006), Article in Press.

[25] Poort, J., Vassilev, A. and Dimitrov, L.: "Did Postglacial Catastrophic Flooding Trigger Massive Changes in the Black Sea Gas Hydrate Reservoir?", *Terra Nova* (2005), Vol. 17, No. 2, 135-140.

[26] Haklıdır, M. and Kapkın, Ş: "Black Sea, A Hydrogen Source*"*, *Proceedings International Hydrogen Energy Congress and Exhibition IHEC 2005*, İstanbul, Turkey, 13-15 July, 2005.

[27] Karabakal, U. and Parlaktuna, M: "*Natural Gas Hydrate Formation Conditions of Black Sea- A Theoretical Approach"* (In Turkish), presented at the 15th International Petroleum and Natural Gas Congress and Exhibition of Turkey IPETGAS 2005, 11-13 May 2005.

[28] Black Sea Database, TU- Black Sea Project (1997), NATO Science for Stability.

[29] Vassilev, A. and Dimitrov, L: "Spatial and Quantity Evalution of the Black Sea Gas Hydrates", *Russian Geol. Geophys.* (2002), 43, 637- 649.

[30] Holger et al.: "Microbial Sulfur Cycle in Black Sea", in *The Black Sea- Geology, Chemistry, and Biology*, Degens, E. T. and Ross, A. D., ed., The American Association of Petroleum Geologists, United States (1974), 419-425.

[31] Korsakov, O. D, Byakov, Y. A. and Stupak, S.: "Gas Hydrates in the Black Sea Basin", *International Geology Review* (1989), 1251-1257.

[32] Parlaktuna, M. and Erdoğmuş, T.: "Natural Gas Hydrate Potential of the Black Sea", *Energy Sources* (2001), 23, 203- 211.

[33] Noaker, J. L. and Katz, L. D.: "Gas Hydrates of Hydrogen Sulfide- Methane Mixtures", *Petroleum Transactions, AIME*, *Journal of Petroleum Technologies* (1954), SPE 367- G, 135-137.

[34] Kastner et al.: "Chemistry, Isotropic Composition, and Origin of a Methane-Hydrogen Sulfide Hydrate at the Cascadia Subduction Zone", *Earth and Planetary Science Letters* (1998), 173-183.

[35] Computer Program "*A_Rate.For"* developed by Parlaktuna, M. and Dogan A. H., 2 February 2002.

[36] Schroeter, J. P. and Kobayashi, R.: "Hydrate Decomposition Conditions in the System H_2S-Methane- Propane", *Ind. Eng. Chem. Fundam.* (1983), 22, 361-364.

[37] Komai, T et al.: "Dynamics of Reformation and Replacement of CO_2 and CH_4 Gas Hydrates", *Annals New York Academy of Sciences* (2000), 912, 272-280.

[38] Oellrich R., L.: "Natural Gas Hydrates and their Potential for Future Energy Supply", *XVII Natural and VI ISHMT/ASME Heat and Mass Transfer Conference, IGCAR,* Kalpakkam, Jan. 5-7, 2004.

APPENDIX A

RESULTS OF THE GAS CHROMOTOGRAPHY REPORTED BY THE TPAO RESEARCH CENTER

TPAO ARAŞTIRMA MERKEZİ
ÜRETİM TEKNOLOJİSİ MÜDÜRLÜĞÜ
GAZ ANALİZ RAPORU

Şirket: ODTÜ/Petrol ve Doğal Gaz Mühendisliği	**Analiz Tarihi:** 16.10.2006
Bölge saha:	**Örnekleme Tarihi:**
Formasyon:	**Derinlik/Aralık (m):**
Sıcaklık (°F):	**Numune Numarası:**
Basınç (psi):	**Örnekleme Yeri:**
Test Sebebi: Gaz Hidrat Projesi Kapsamında Yapılan Analiz	

Bileşenler		Mol, %	Ölçüm Belirsizliği (±)	Yöntem ASTM D-1945
H_2	Hidrojen	2,144	0,055	
Ar	Argon	0,987	0,026	
N_2	Azot	6,987	0,181	
CO_2	Karbondioksit	0,000	-	
C_1	Metan	89,873	2,322	
C_2	Etan	0,009	0,000	
C_3	Propan	0,000	-	
iC_4	iso-Butan	0,000	-	
nC_4	n-Butan	0,000	-	
iC_5	iso-Pentan	0,000	-	
nC_5	n-Pentan	0,000	-	
nC_6	n-Hekzan	0,000	-	
Toplam		100		
*Diğer Sülfür Bileşikleri		ppm		
H_2S	Hidrojen Sülfür	128,8145	0,001	
COS	Karbonil Sülfür	0	-	
CH_3SH	Metil Merkaptan	0,95147	0,000	
C_2H_5SH	Etil Merkaptan	0	-	

Bazı Gaz Özellikleri:			ISO 6976
Pseudo Kritik Basınç,psia	:	644,9	
Pseudo Kritik Sıcaklık,°R	:	328,1	
Mol Ağırlık,g/mol	:	16,816	
Özgül Ağırlık (25 °C-1 atm)	:	0,581	
Üst Isı Değeri,kcal/sm^3	:	8173,43	
Alt Isı Değeri,kcal/sm^3	:	7355,39	
Wobbe Sayısı,kcal/sm^3	:	10720	
Sıkıştırma Faktörü	:	0,9983	

Figure A.1- The Result of the Gas Chromotography (129 ppm) for the Experiment Group I

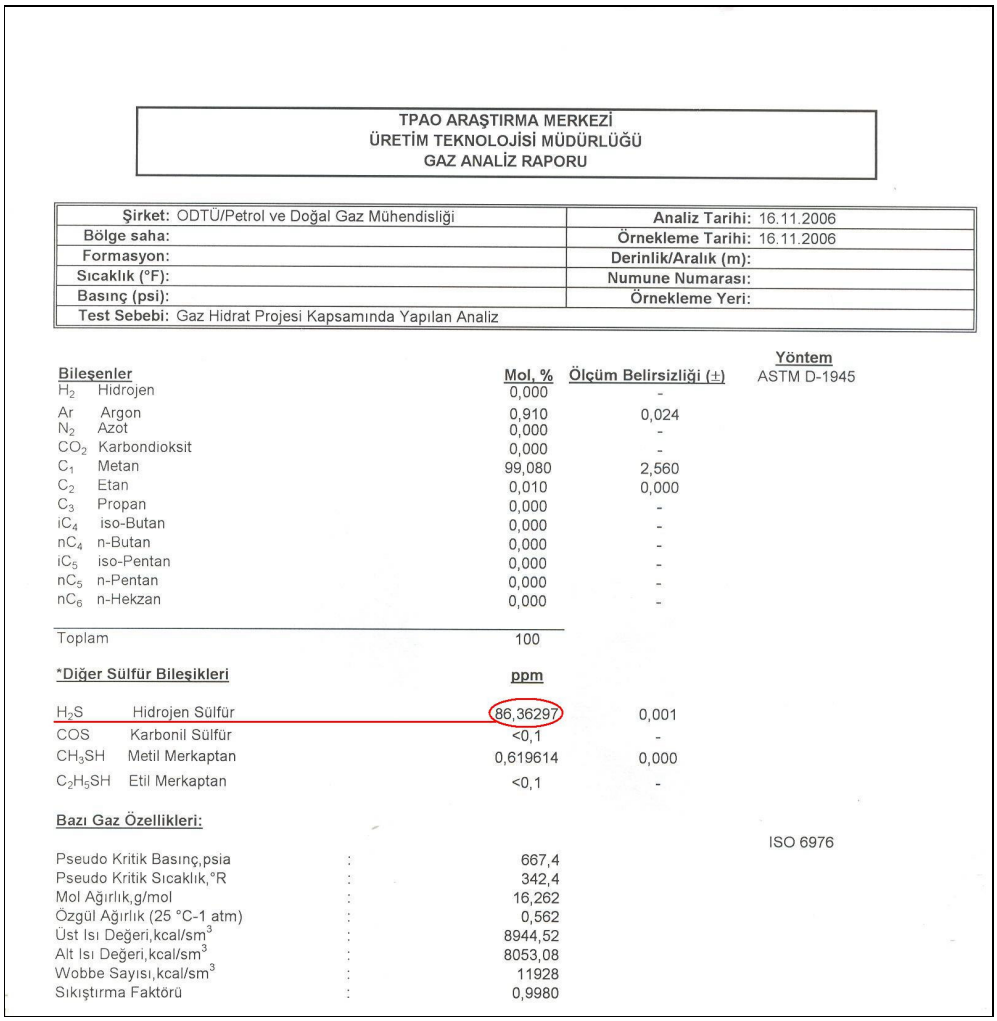

TPAO ARAŞTIRMA MERKEZİ
ÜRETİM TEKNOLOJİSİ MÜDÜRLÜĞÜ
GAZ ANALİZ RAPORU

Şirket: ODTÜ/Petrol ve Doğal Gaz Mühendisliği	**Analiz Tarihi:** 16.11.2006
Bölge saha:	**Örnekleme Tarihi:** 16.11.2006
Formasyon:	**Derinlik/Aralık (m):**
Sıcaklık (°F):	**Numune Numarası:**
Basınç (psi):	**Örnekleme Yeri:**
Test Sebebi: Gaz Hidrat Projesi Kapsamında Yapılan Analiz	

Bileşenler		Mol, %	Ölçüm Belirsizliği (±)	Yöntem
H_2	Hidrojen	0,000	-	ASTM D-1945
Ar	Argon	0,910	0,024	
N_2	Azot	0,000	-	
CO_2	Karbondioksit	0,000	-	
C_1	Metan	99,080	2,560	
C_2	Etan	0,010	0,000	
C_3	Propan	0,000	-	
iC_4	iso-Butan	0,000	-	
nC_4	n-Butan	0,000	-	
iC_5	iso-Pentan	0,000	-	
nC_5	n-Pentan	0,000	-	
nC_6	n-Hekzan	0,000	-	
Toplam		100		

*Diğer Sülfür Bileşikleri		ppm		
H_2S	Hidrojen Sülfür	86,36297	0,001	
COS	Karbonil Sülfür	<0,1	-	
CH_3SH	Metil Merkaptan	0,619614	0,000	
C_2H_5SH	Etil Merkaptan	<0,1	-	

Bazı Gaz Özellikleri:

Pseudo Kritik Basınç,psia	:	667,4	ISO 6976
Pseudo Kritik Sıcaklık,°R	:	342,4	
Mol Ağırlık,g/mol	:	16,262	
Özgül Ağırlık (25 °C-1 atm)	:	0,562	
Üst Isı Değeri,kcal/sm^3	:	8944,52	
Alt Isı Değeri,kcal/sm^3	:	8053,08	
Wobbe Sayısı,kcal/sm^3	:	11928	
Sıkıştırma Faktörü	:	0,9980	

Figure A.2- The Result of the Gas Chromotography (86 ppm) for the Experiment Group II

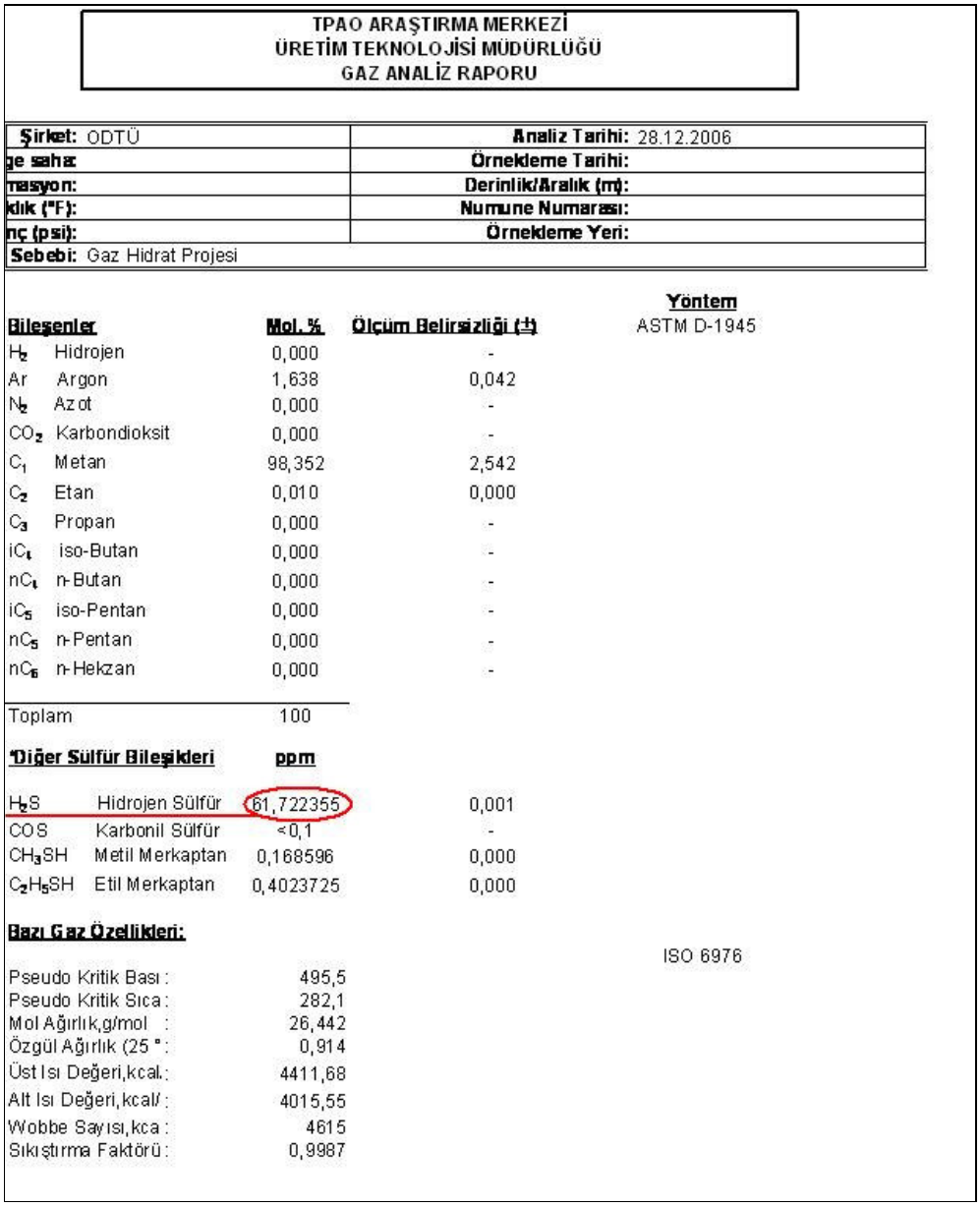

TPAO ARAŞTIRMA MERKEZİ
ÜRETİM TEKNOLOJİSİ MÜDÜRLÜĞÜ
GAZ ANALİZ RAPORU

Şirket: ODTÜ	**Analiz Tarihi:** 28.12.2006
ge saha:	**Örnekleme Tarihi:**
nasyon:	**Derinlik/Aralık (m):**
kık (°F):	**Numune Numarası:**
nç (psi):	**Örnekleme Yeri:**
Sebebi: Gaz Hidrat Projesi	

Bileşenler		**Mol. %**	**Ölçüm Belirsizliği (±)**	**Yöntem** ASTM D-1945
H_2	Hidrojen	0,000	-	
Ar	Argon	1,638	0,042	
N_2	Azot	0,000	-	
CO_2	Karbondioksit	0,000	-	
C_1	Metan	98,352	2,542	
C_2	Etan	0,010	0,000	
C_3	Propan	0,000	-	
iC_4	iso-Butan	0,000	-	
nC_4	n-Butan	0,000	-	
iC_5	iso-Pentan	0,000	-	
nC_5	n-Pentan	0,000	-	
nC_6	n-Hekzan	0,000	-	
Toplam		100		

Diğer Sülfür Bileşikleri		**ppm**	
H_2S	Hidrojen Sülfür	61,722355	0,001
COS	Karbonil Sülfür	<0,1	-
CH_3SH	Metil Merkaptan	0,168596	0,000
C_2H_5SH	Etil Merkaptan	0,4023725	0,000

Bazı Gaz Özellikleri: ISO 6976

Pseudo Kritik Bası :	495,5
Pseudo Kritik Sıca :	282,1
Mol Ağırlık,g/mol :	26,442
Özgül Ağırlık (25 ° :	0,914
Üst Isı Değeri,kcal :	4411,68
Alt Isı Değeri,kcal/ :	4015,55
Wobbe Sayısı,kca :	4615
Sıkıştırma Faktörü :	0,9987

Figure A.3- The Result of the Gas Chromotography (62 ppm) for the Experiment Group III

APPENDIX B

PRESSURE-TEMPERATURE VS. TIME PLOTS OF THE EXPERIMENTS

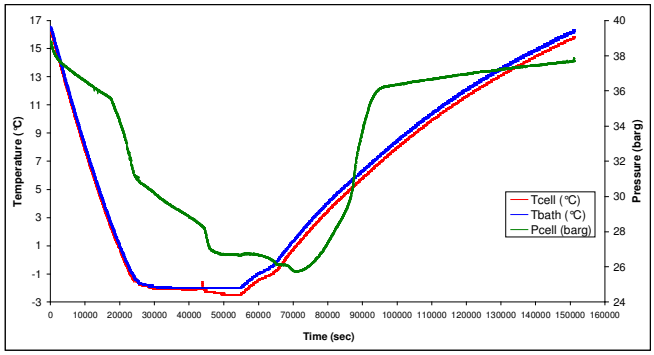

Figure B.1- Pressure-Temperature-Time Plot of the Experiment I-1

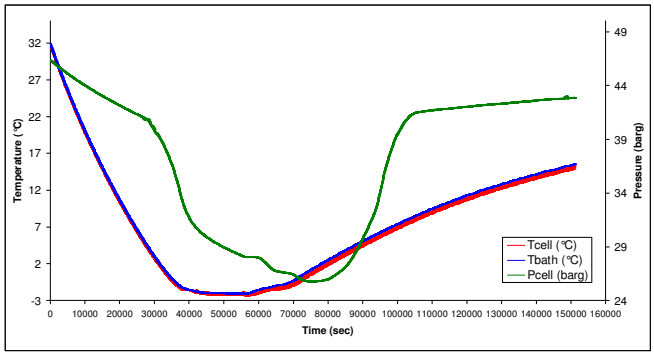

Figure B.2- Pressure-Temperature-Time Plot of the Experiment I-2

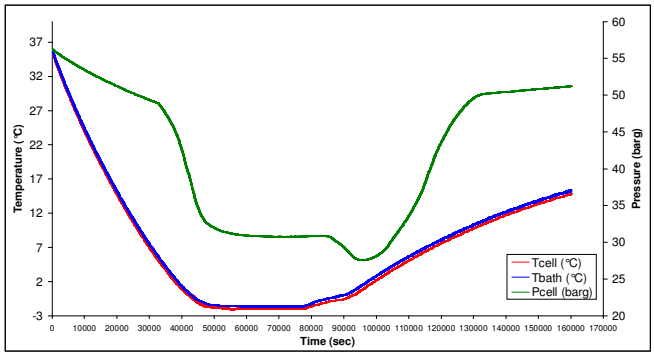

Figure B.3- Pressure-Temperature-Time Plot of the Experiment I-3

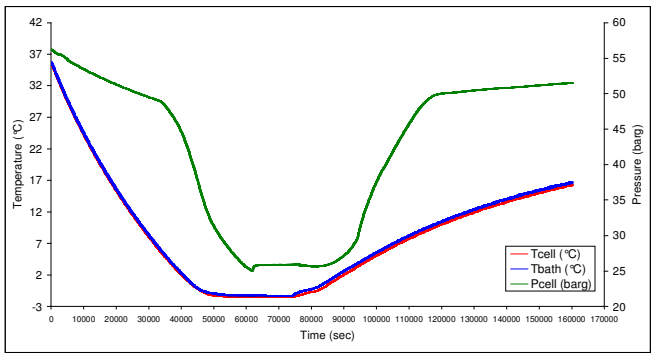

Figure B.4- Pressure-Temperature-Time Plot of the Experiment I-4

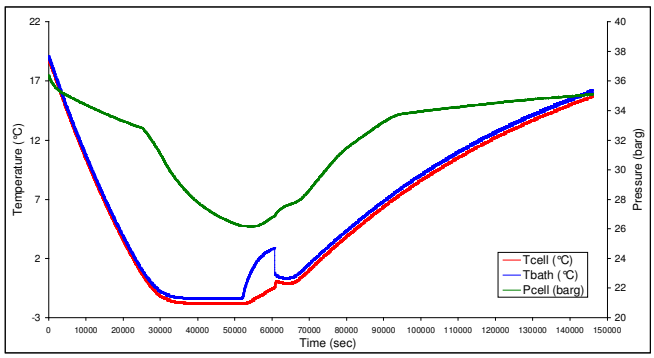

Figure B.5- Pressure-Temperature-Time Plot of the Experiment I-5

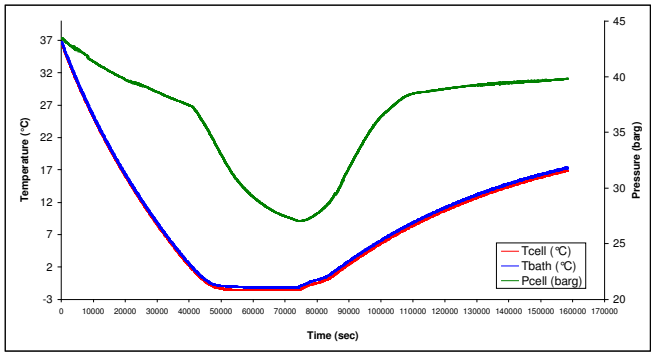

Figure B.6- Pressure-Temperature-Time Plot of the Experiment I-6

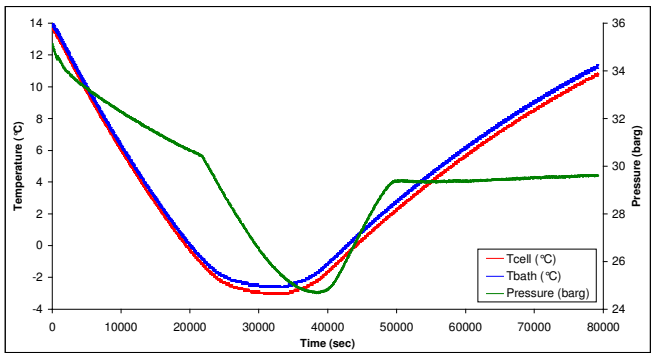

Figure B.7- Pressure-Temperature-Time Plot of the Experiment II-1

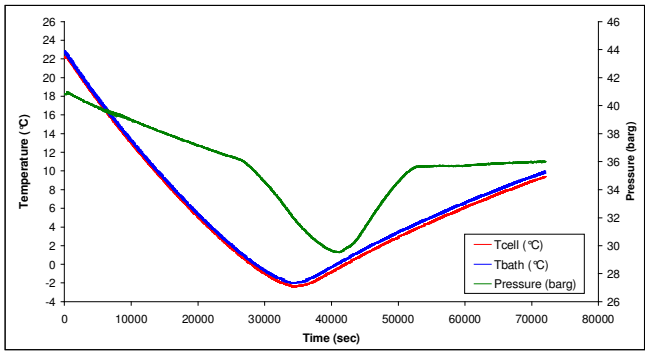

Figure B.8- Pressure-Temperature-Time Plot of the Experiment II-2

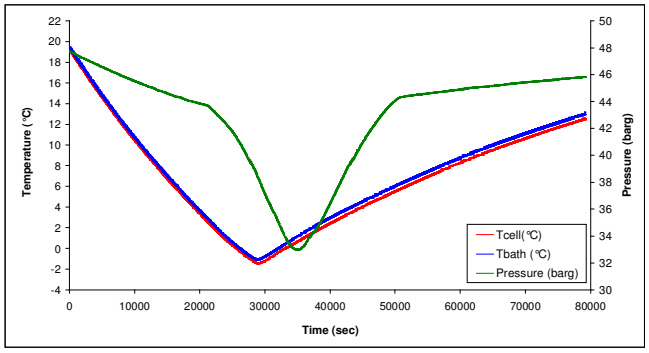

Figure B.9- Pressure-Temperature-Time Plot of the Experiment II-3

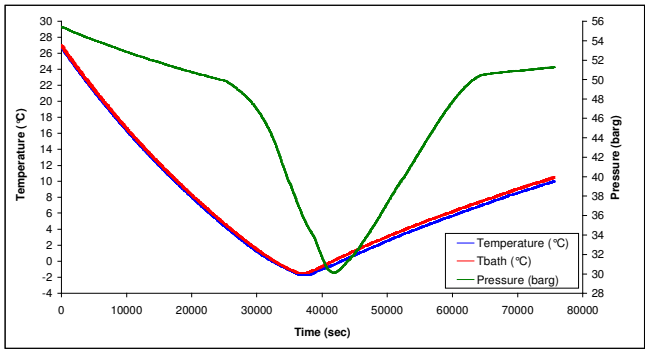

Figure B.10- Pressure-Temperature-Time Plot of the Experiment II-4

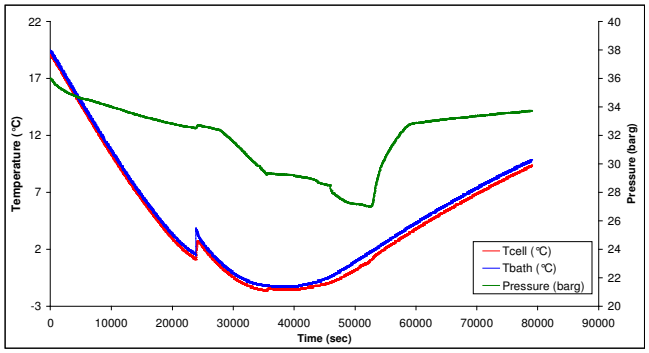

Figure B.11- Pressure-Temperature-Time Plot of the Experiment II-5

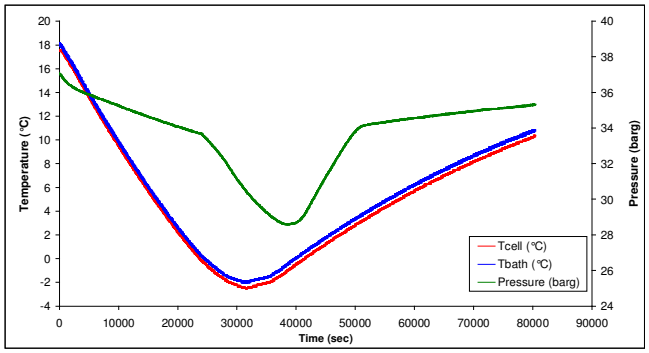

Figure B.12- Pressure-Temperature-Time Plot of the Experiment III-1

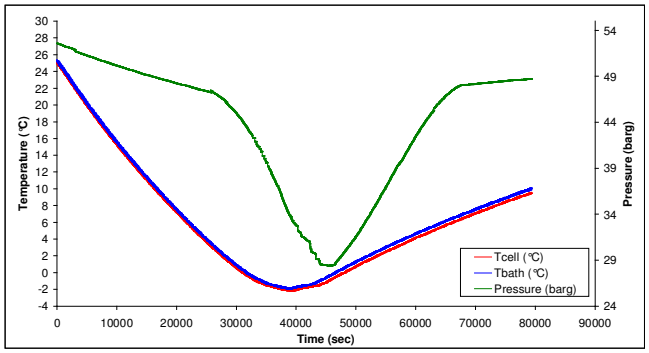

Figure B.13- Pressure-Temperature-Time Plot of the Experiment III-2

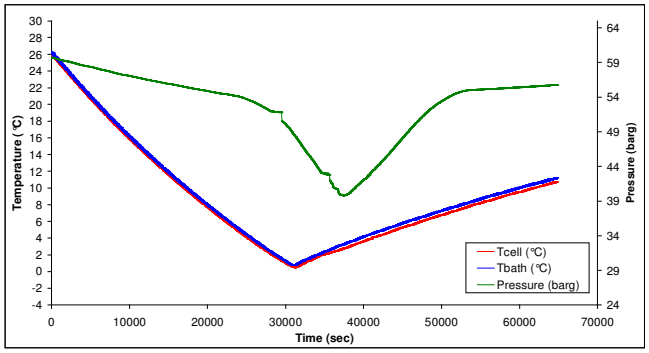

Figure B.14- Pressure-Temperature-Time Plot of the Experiment III-3

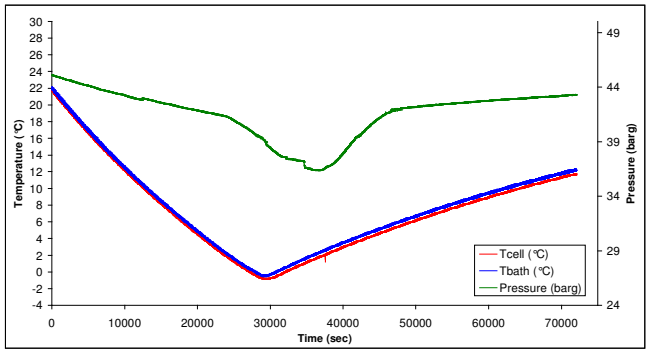

Figure B.15- Pressure-Temperature-Time Plot of the Experiment III-4

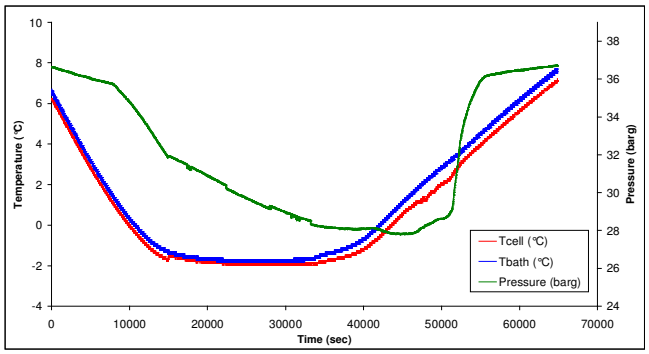

Figure B.16- Pressure-Temperature-Time Plot of the Experiment III-5

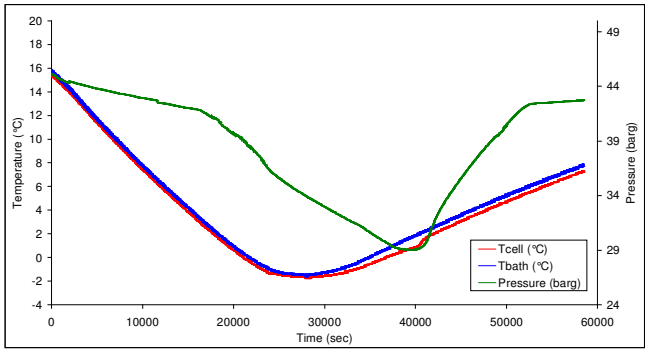

Figure B.17- Pressure-Temperature-Time Plot of the Experiment III-6

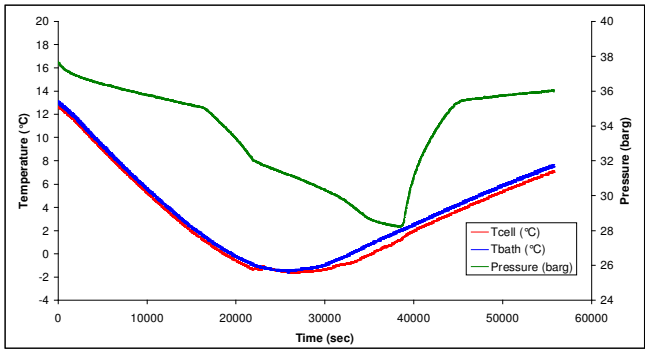

Figure B.18- Pressure-Temperature-Time Plot of the Experiment III-7

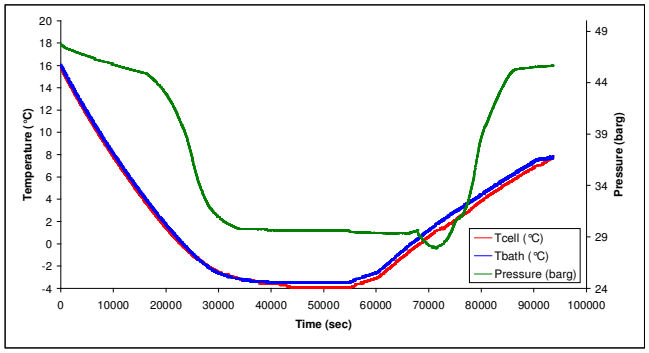

Figure B.19- Pressure-Temperature-Time Plot of the Experiment IV-1

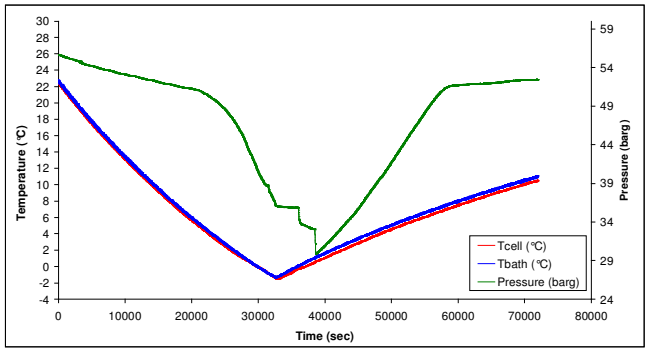

Figure B.20- Pressure-Temperature-Time Plot of the Experiment IV-2

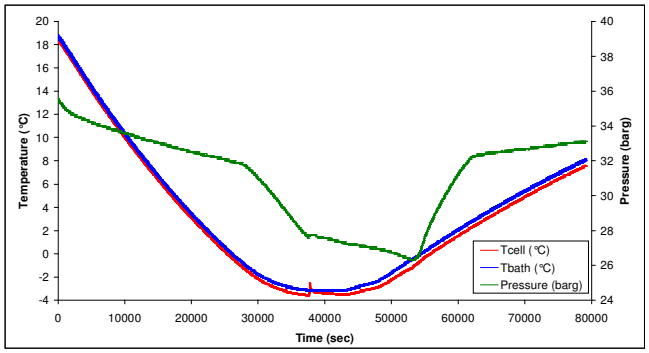

Figure B.21- Pressure-Temperature-Time Plot of the Experiment IV-3

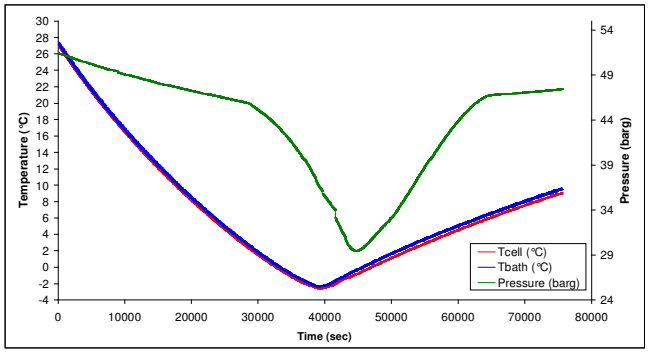

Figure B.22- Pressure-Temperature-Time Plot of the Experiment IV-4

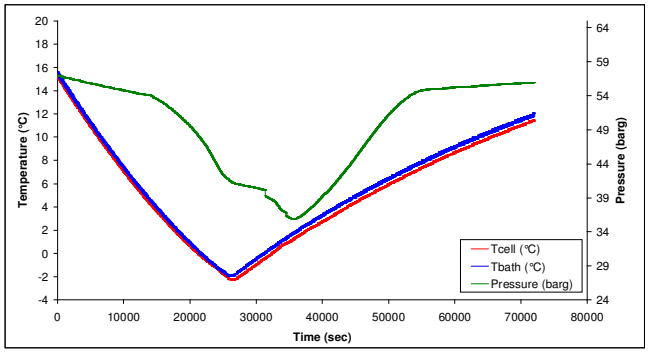

Figure B.23- Pressure-Temperature-Time Plot of the Experiment IV-5

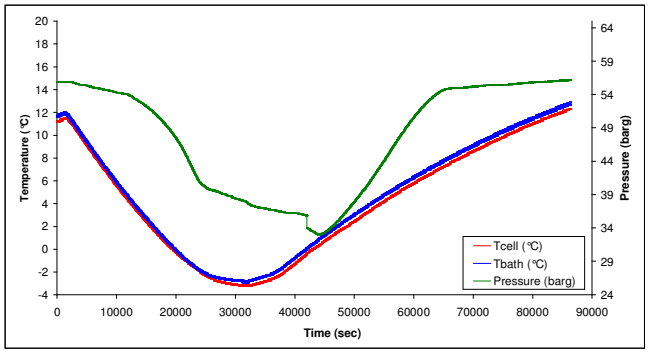

Figure B.24- Pressure-Temperature-Time Plot of the Experiment IV-6

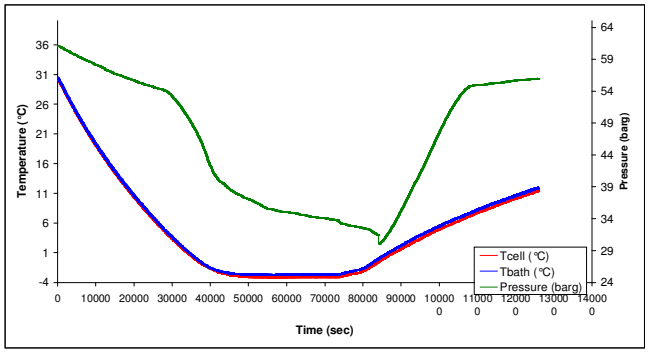

Figure B.25- Pressure-Temperature-Time Plot of the Experiment IV-7

APPENDIX C

PRESSURE vs. TEMPERATURE PLOTS OF THE EXPERIMENTS

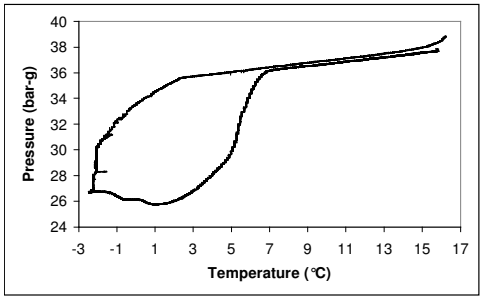

Figure C.1- Pressure-Temperature Plot of the Experiment I-1

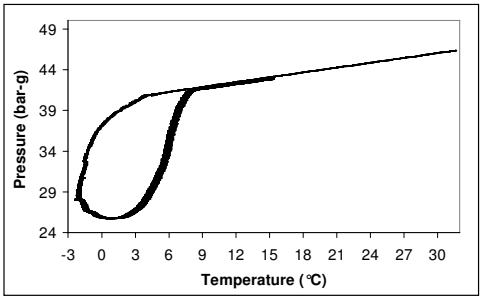

Figure C.2- Pressure-Temperature Plot of the Experiment I-2

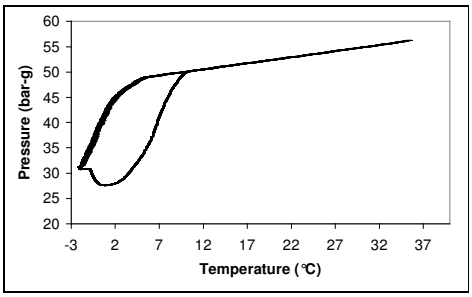

Figure C.3- Pressure-Temperature Plot of the Experiment I-3

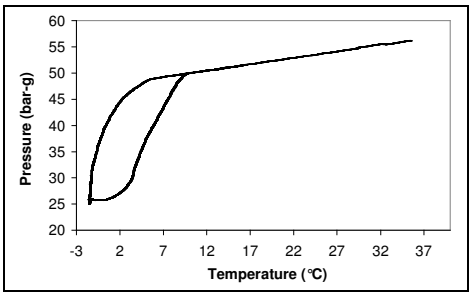

Figure C.4- Pressure-Temperature Plot of the Experiment I-4

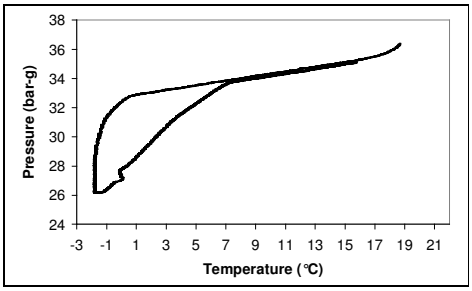

Figure C.5- Pressure-Temperature Plot of the Experiment I-5

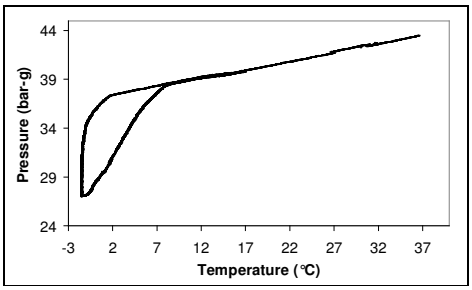

Figure C.6- Pressure-Temperature Plot of the Experiment I-6

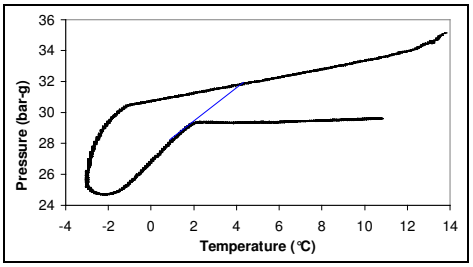

Figure C.7- Pressure-Temperature Plot of the Experiment II-1

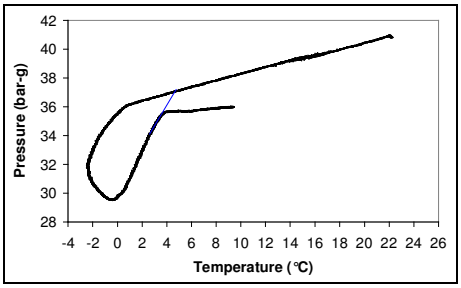

Figure C.8- Pressure-Temperature Plot of the Experiment II-2

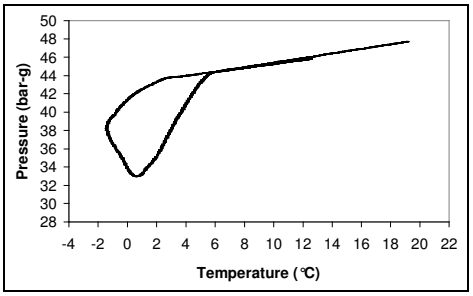

Figure C.9- Pressure-Temperature Plot of the Experiment II-3

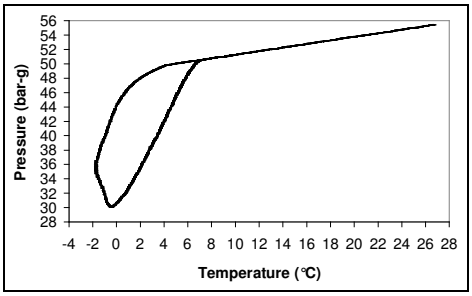

Figure C.10- Pressure-Temperature Plot of the Experiment II-4

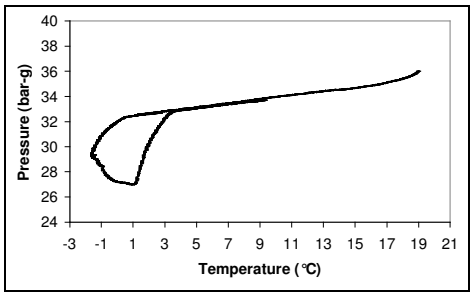

Figure C.11- Pressure-Temperature Plot of the Experiment II-5

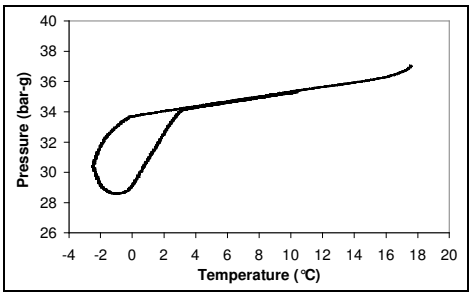

Figure C.12- Pressure-Temperature Plot of the Experiment III-1

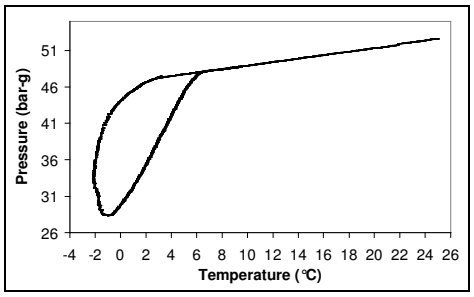

Figure C.13- Pressure-Temperature Plot of the Experiment III-2

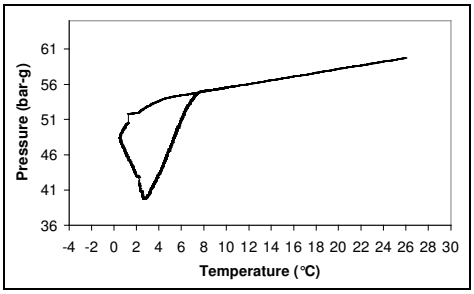

Figure C.14- Pressure-Temperature Plot of the Experiment III-3

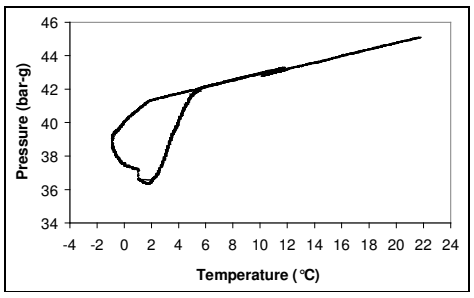

Figure C.15- Pressure-Temperature Plot of the Experiment III-4

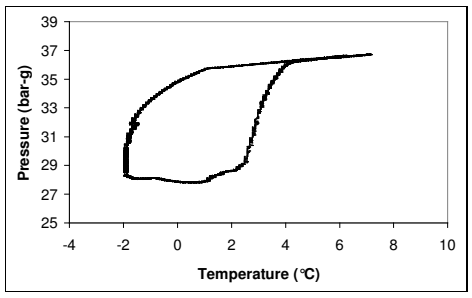

Figure C.16- Pressure-Temperature Plot of the Experiment III-5

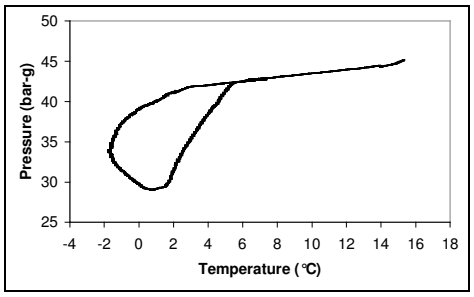

Figure C.17- Pressure-Temperature Plot of the Experiment III-6

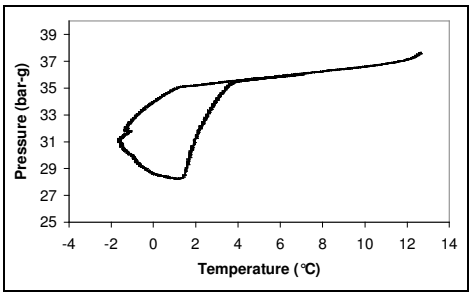

Figure C.18- Pressure-Temperature Plot of the Experiment III-7

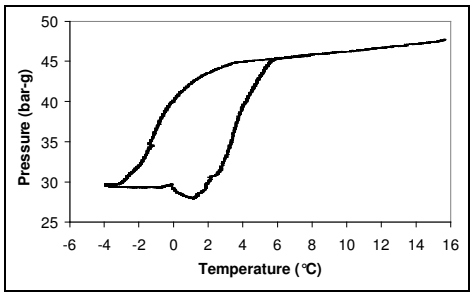

Figure C.19- Pressure-Temperature Plot of the Experiment IV-1

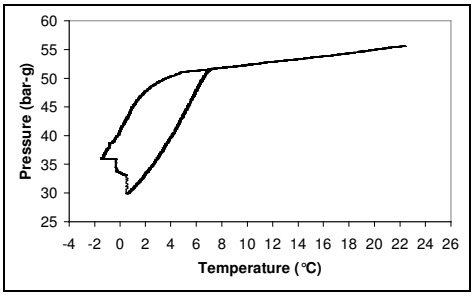

Figure C.20- Pressure-Temperature Plot of the Experiment IV-2

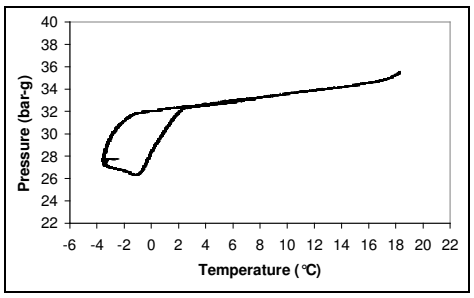

Figure C.21- Pressure-Temperature Plot of the Experiment IV-3

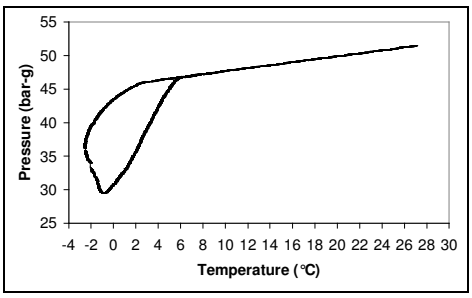

Figure C.22- Pressure-Temperature Plot of the Experiment IV-4

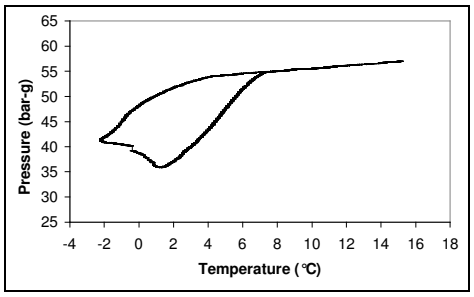

Figure C.23- Pressure-Temperature Plot of the Experiment IV-5

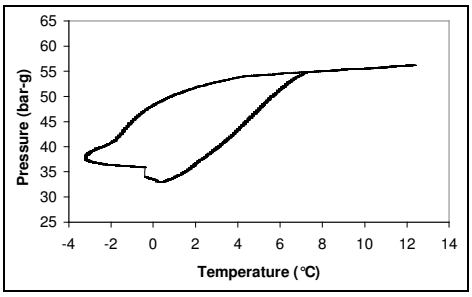

Figure C.24- Pressure-Temperature Plot of the Experiment IV-6

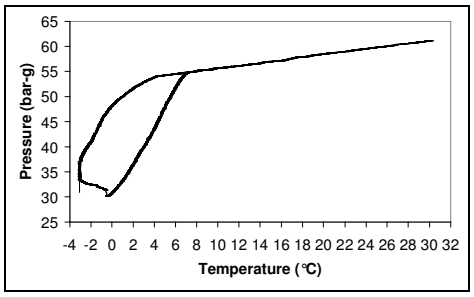

Figure C.25- Pressure-Temperature Plot of the Experiment IV-7

APPENDIX D

NUMBER OF MOLES OF FREE GAS VS. TIME PLOTS OF THE EXPERIMENTS

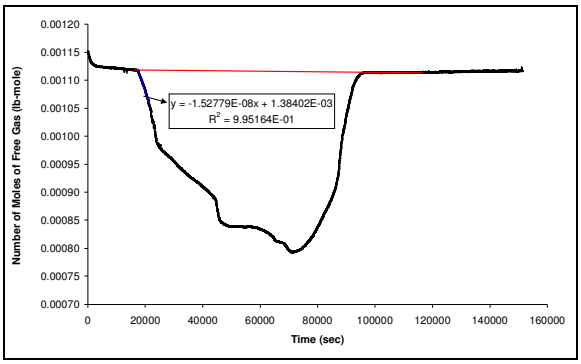

Figure D.1- Number of Moles of Free Gas- Time Plot (I-1)

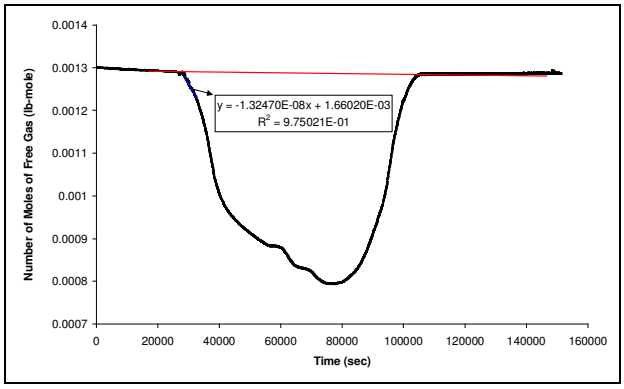

Figure D.2- Number of Moles of Free Gas- Time Plot (I-2)

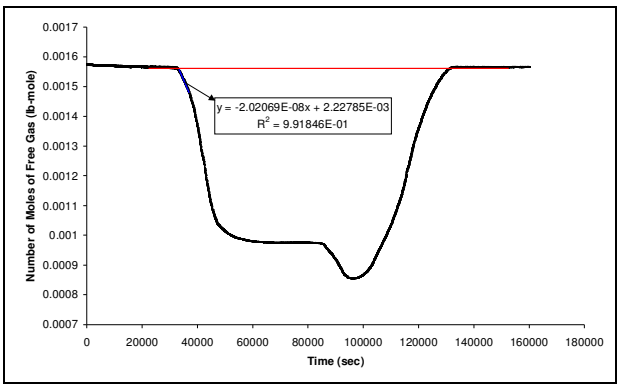

Figure D.3- Number of Moles of Free Gas- Time Plot (I-3)

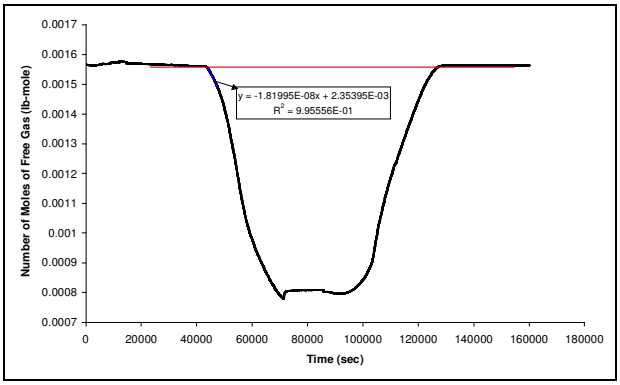

Figure D.4- Number of Moles of Free Gas- Time Plot (I-4)

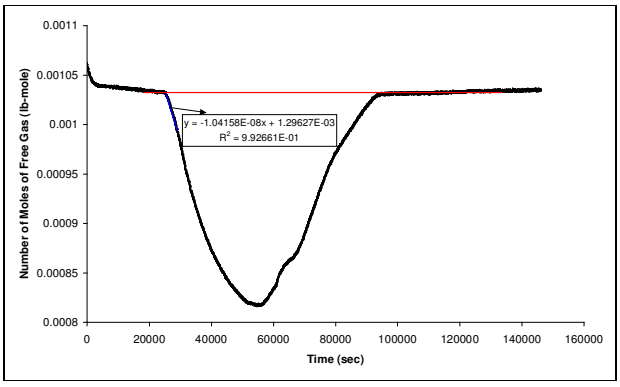

Figure D.5- Number of Moles of Free Gas- Time Plot (I-5)

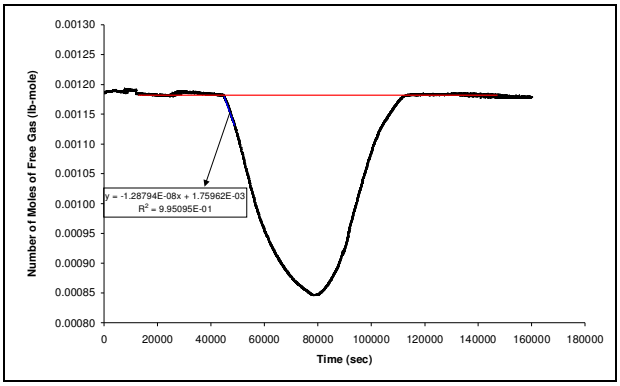

Figure D.6- Number of Moles of Free Gas- Time Plot (I-6)

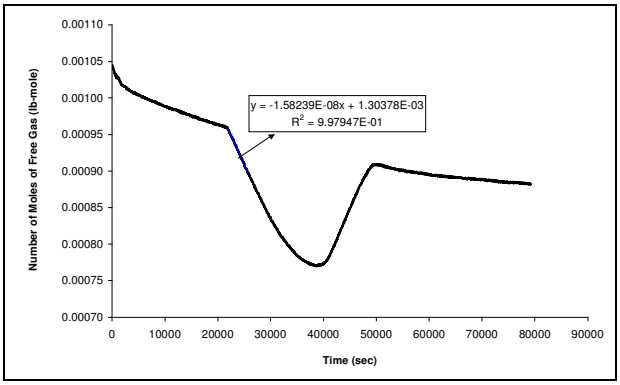

Figure D.7- Number of Moles of Free Gas- Time Plot (II-1)

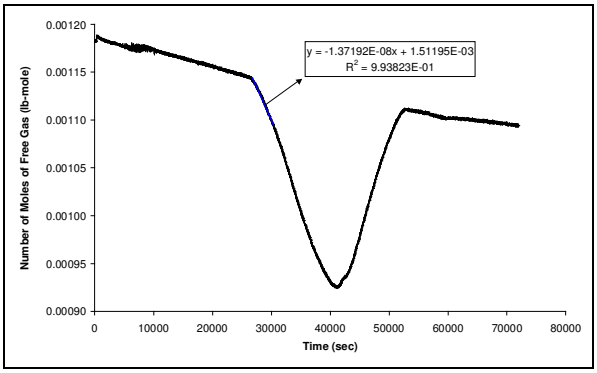

Figure D.8- Number of Moles of Free Gas- Time Plot (II-2)

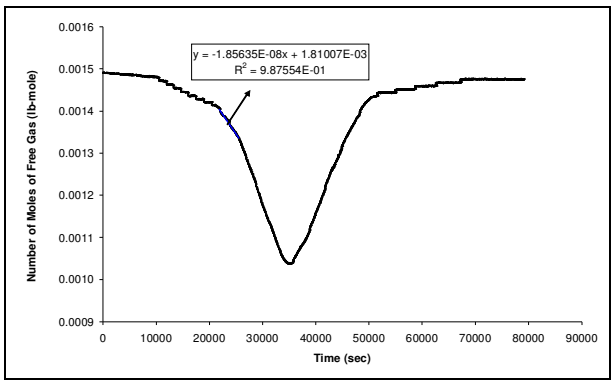

Figure D.9- Number of Moles of Free Gas- Time Plot (II-3)

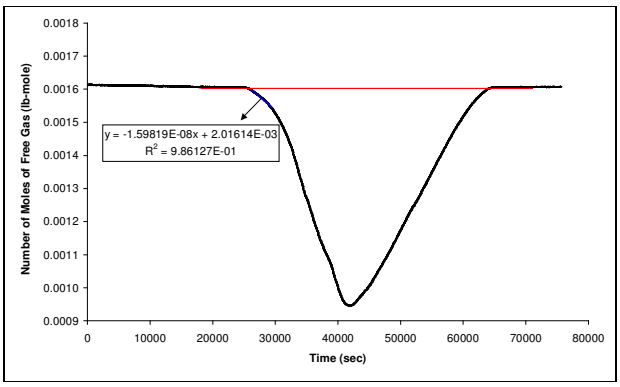

Figure D.10- Number of Moles of Free Gas- Time Plot (II-4)

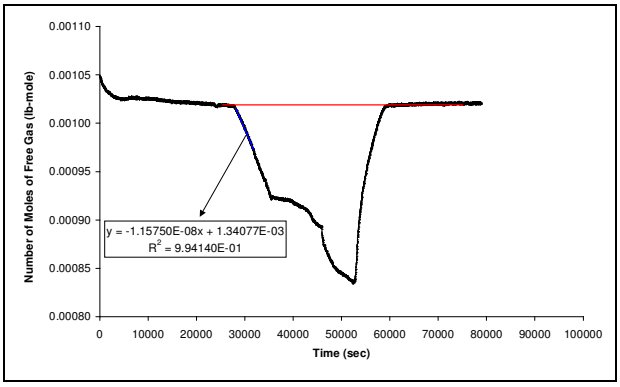

Figure D.11- Number of Moles of Free Gas- Time Plot (II-5)

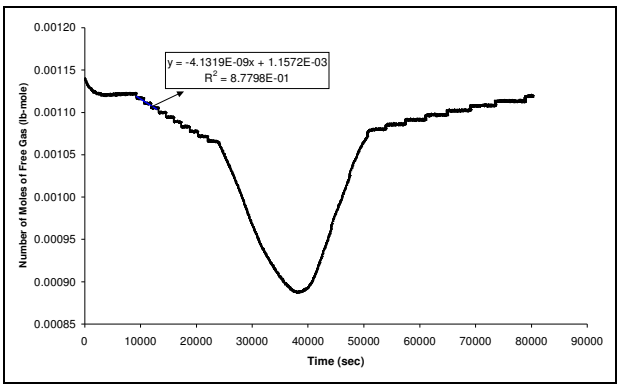

Figure D.12- Number of Moles of Free Gas- Time Plot (III-1)

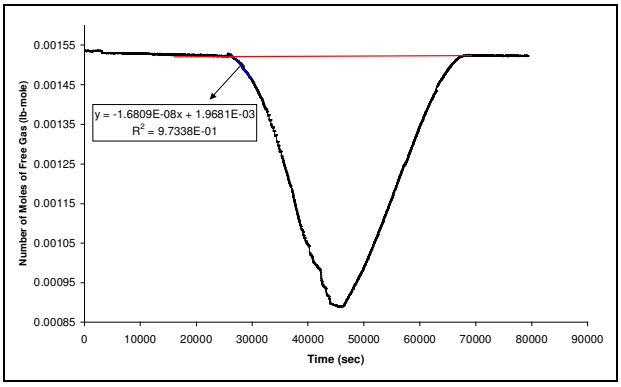

Figure D.13- Number of Moles of Free Gas- Time Plot (III-2)

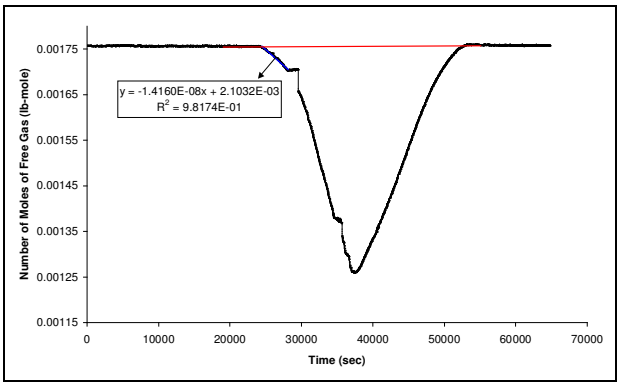

Figure D.14- Number of Moles of Free Gas- Time Plot (III-3)

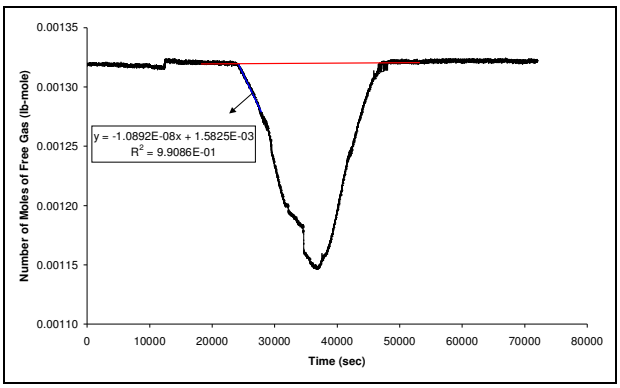

Figure D.15- Number of Moles of Free Gas- Time Plot (III-4)

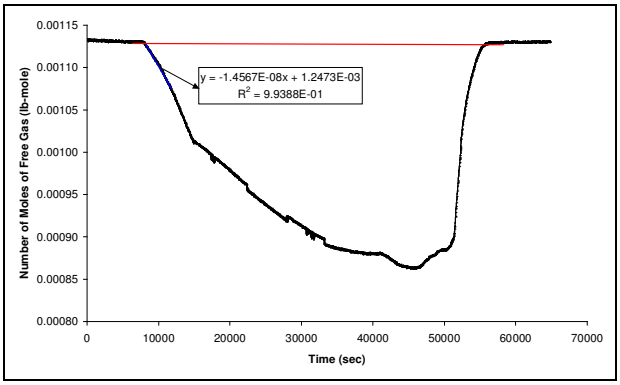

Figure D.16- Number of Moles of Free Gas- Time Plot (III-5)

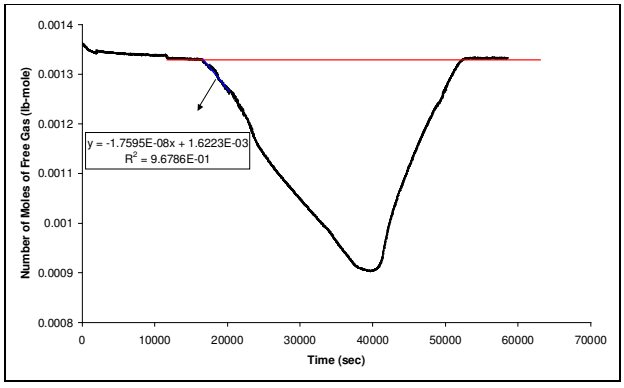

Figure D.17- Number of Moles of Free Gas- Time Plot (III-6)

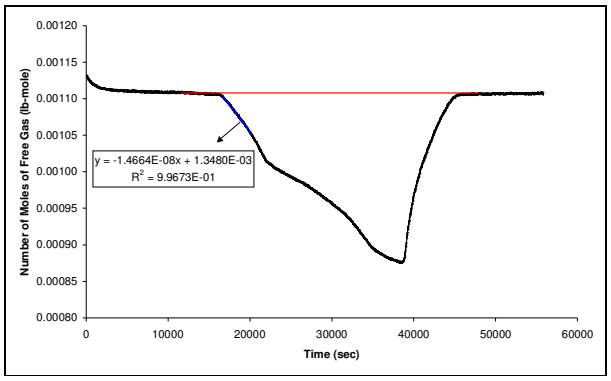

Figure D.18- Number of Moles of Free Gas- Time Plot (III-7)

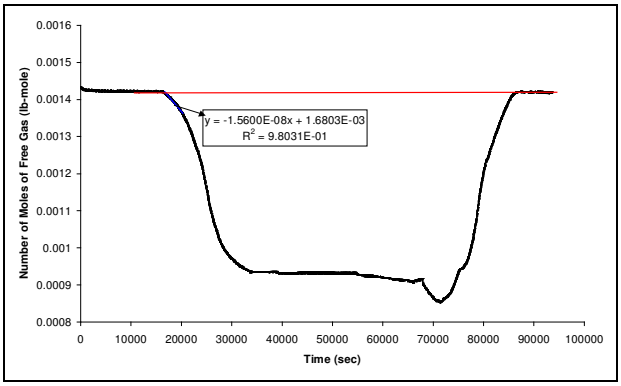

Figure D.19- Number of Moles of Free Gas- Time Plot (IV-1)

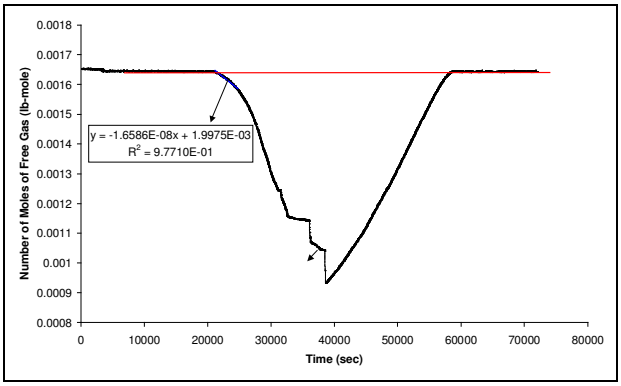

Figure D.20- Number of Moles of Free Gas- Time Plot (IV-2)

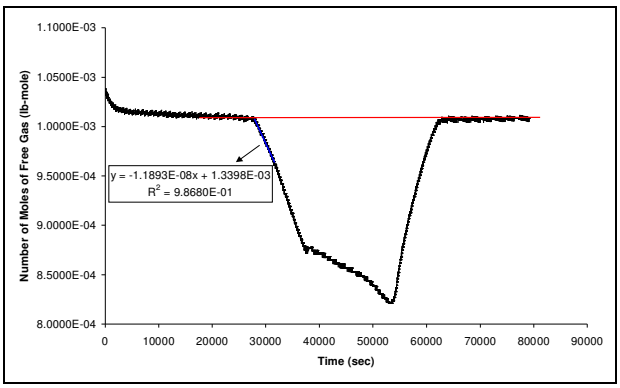

Figure D.21- Number of Moles of Free Gas- Time Plot (IV-3)

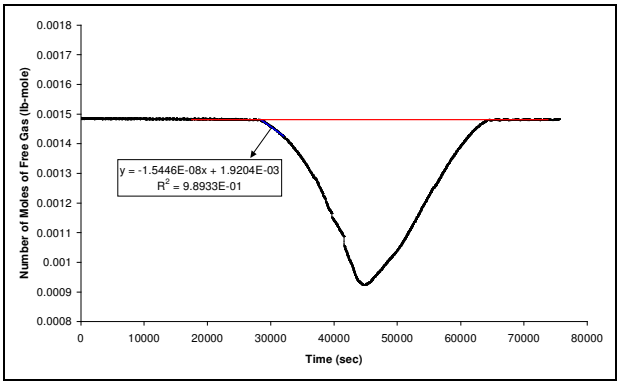

Figure D.22- Number of Moles of Free Gas- Time Plot (IV-4)

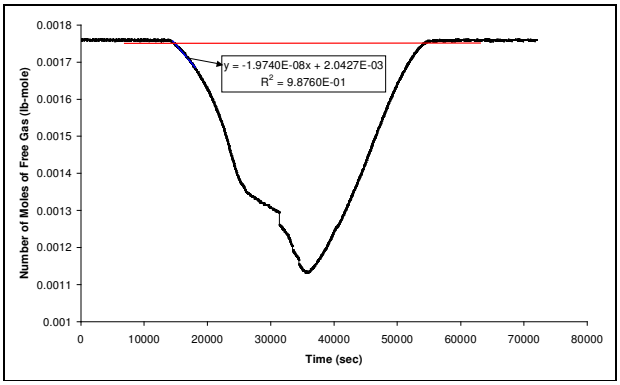

Figure D.23- Number of Moles of Free Gas- Time Plot (IV-5)

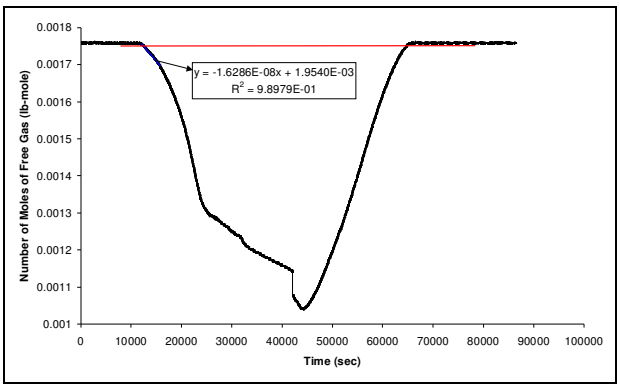

Figure D.24- Number of Moles of Free Gas- Time Plot (IV-6)

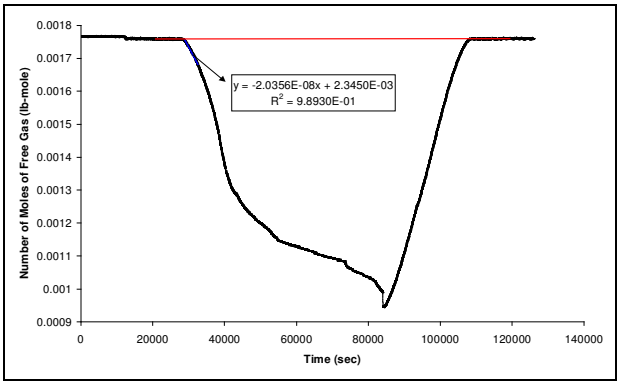

Figure D.25- Number of Moles of Free Gas- Time Plot (IV-7)

APPENDIX E

UNIT CONVERSION BETWEEN PPM AND MOLE PER CENT FOR 129, 86, 62 PPM H_2S CONCENTRATION

- Converting 129 ppm to mole %: (129 ppm= 0.0129 % wt/wt)

Table E.1- Conversion Between ppm and Mole Per cent for 129 ppm H_2S Concentration

	(1)	(2)	(3)	(4)	(5)	(6)	(7)	(8)
Com	Mole, %	Mole, Frac	Molecular weight, g/g-mole	Mass, g	Mass, in 100 g	Mass, in (100-0.0129) g	Mole	Mole, %
H_2	2.144	0.0214	2.02	0.043	0.2576	0.2576	0.1275	2.1439
Ar	0.987	0.0099	39.95	0.394	2.3452	2.3449	0.0587	0.9869
N_2	6.987	0.0699	28.01	1.957	11.6401	11.6386	0.4155	6.9866
C_1	89.87	0.8987	16.04	14.42	85.7409	85.7299	5.3448	89.867
C_2	0.009	0.0001	30.07	0.003	0.0161	0.01609	0.00054	**0.0064**
H_2S			34.08		0.0129		0.00038	
Total	100	1		16.81	100.013	99.871	5.9474	100

(1): Results of Gas Chromatography Reported by TPAO.

(4) = (2) × (3)

(5) = 100 × (4) / 16.813

(6) = (100-0.0129) × (5) /100

(7) = (6) / (3)

(8) = 100 × (7)/ 5.9474

129 ppm = 0.0064 mole %

- Converting 86 ppm to mole %: (86 ppm= 0.0086 % wt/wt)

Table E.2- Conversion Between ppm and Mole Per cent for 86 ppm H_2S Concentration

	(1)	(2)	(3)	(4)	(5)	(6)	(7)	(8)
Com.	Mole, %	Mole, Frac	Molecular weight, g/g-mole	Mass, g	Mass, in 100 g	Mass, in (100-0.0086) g	Mole	Mole, %
Ar	0.910	0.0091	39.95	0.364	2.2360	2.2358	0.0560	0.9100
C_1	99.08	0.9908	16.04	15.89	97.7455	97.7371	6.0933	99.076
C_2	0.010	0.0001	30.07	0.003	0.0185	0.01849	0.00061	0.0100
H_2S			34.08		0.0086		0.00025	**0.0041**
Total	100	1		16.26	100.008	99.991	6.150	100

(1): Results of Gas Chromatography Reported by TPAO.

(4) = (2) × (3)

(5) = 100 × (4) / 16.259

(6) = (100-0.0086) × (5) /100

(7) = (6) / (3)

(8) = 100 × (7)/ 6.150

86 ppm = 0.0041 mole %

- Converting 62 ppm to mole %: (62 ppm= 0.0062 % wt/wt)

Table E.3- Conversion Between ppm and Mole Per cent for 62 ppm H_2S Concentration

	(1)	(2)	(3)	(4)	(5)	(6)	(7)	(8)
Com	Mole, %	Mole, Frac	Molecular weight, g/g-mole	Mass, g	Mass, in 100 g	Mass, in (100-0.0062) g	Mole	Mole, %
Ar	1.638	0.0164	39.95	0.654	3.9821	3.9819	0.0997	1.638
C_1	98.35	0.9835	16.04	15.78	95.9996	95.9936	5.9846	98.35
C_2	0.010	0.0001	30.07	0.003	0.0183	0.01830	0.00061	0.010
H_2S			34.08		0.0062		0.00018	**0.0030**
Total	100	1		16.43	100.006	99.994	6.085	100

(1): Results of Gas Chromatography Reported by TPAO.

(4) = (2) × (3)

(5) = 100 × (4) / 16.433

(6) = (100-0.0062) × (5) /100

(7) = (6) / (3)

(8) = 100 × (7)/ 6.085

62 ppm = 0.0030 mole %